

# The Disc Accretion in Gravitational Field of a Rapidly Rotating Neutron Star with a Rotationally Induced Quadrupole Mass Distribution

The paper is accepted by *Astronomy Letters*, v.24, p.894, 1998

N. R. Sibgatullin<sup>1,3</sup> and R. A. Sunyaev<sup>2,3</sup>

<sup>1</sup> Moscow State University, Faculty of Mech. & Math., Moscow, 119899 Russia

<sup>2</sup> Space Research Institute, Russian Academy of Sciences, ul. Profsoyuznaya 84/32, Moscow, 117810 Russia

<sup>3</sup> Max-Planck Institut fuer Astrophysik, Garching, Germany

**Abstract** We analyze the effect of the quadrupole component in the mass distribution of a rapidly rotating neutron star on energy release in the boundary layer on the surface of the accreting star and in the accretion disk in the cases where the stellar radius is smaller (or larger) than the radius of the marginally stable circular orbit. We calculate the velocities and trajectories of the particles that fall on the stellar surface from the marginally stable orbit for a low-luminosity accreting source. The corresponding external gravitational field of the star is modeled by a new exact solution of the Einstein equations in vacuum. The parameters of this solution are adjusted by reconciling the numerical data for the radius of the marginally stable orbit and the gravitational redshift of Cook et al. (1994) with the corresponding data in the analytical solution. For various equations of state, we consider  $1.4M_{\odot}$  normal sequences and maximum mass normal sequences.

## Introduction

The discovery of quasi-periodic oscillations (QPOs) with a frequency 1 kHz from several low-mass X-ray binaries and X-ray bursters has again attracted attention to the detailed theory of disk accretion onto neutron stars with weak magnetic fields. RXTE observations have clearly revealed accreting neutron stars with rotation periods of several milliseconds. There is no doubt that these objects emit through disk accretion, but so far no detailed theory has been developed that would fully explain their observed spectra. For a high luminosity  $L > 0.05L_{\text{edd}}$ , this problem requires a proper allowance for the inverse effect of radiation pressure on the trajectories of particles and on the shape of the disk and the boundary layer. In the low-luminosity limit  $L \ll 0.05L_{\text{edd}}$ , the inverse effect of radiation pressure can be ignored, and we can estimate the relative contributions of the disk and the boundary layer. Below,  $L_{\text{edd}}$  denotes the critical Eddington stellar luminosity.

In the Newtonian theory of disk accretion onto a *nonrotating* star with no magnetic

field, one half of the gravitational energy of accreted particles is liberated in an extended disk, and the other half converts into radiation and heat in a narrow equatorial layer around the star where the particle velocity decreases from the Keplerian velocity to the velocity of the star’s outer layer.

For a *rotating* star in the Newtonian theory, the maximum energy that can be liberated in the boundary layer is proportional to the square of the difference between the angular velocities of particles in a Keplerian orbit with a radius close to the stellar radius and the stellar angular velocity  $\Omega$ :  $\frac{1}{2}(\Omega_K - \Omega)^2 R^2 \dot{M} = \frac{1}{2} G \dot{M} (1 - \Omega/\Omega_K)^2 / R$ . , while the energy released in the disk does not depend on whether the neutron star rotates or not.

Granat, RXTE, and GRO observations of several X-ray bursters have shown that their spectra are highly variable and that hard tails occasionally appear in their spectra up to energies 100 keV. It is tempting to explain such hard tails by the emission from particles that break loose from the last stable orbit and fall on the stellar surface at a great velocity.

These two experimental facts (the discovery of QPOs and of hard X-ray emission from neutron stars) have prompted us to return to the problem that was stated by Sunyaev and Shakura (1986). These authors pointed out that the neutron-star radius could be appreciably *smaller* than the radius of the marginally stable orbit. In this case, the accretion disk can extend only to the radius of the marginally stable orbit. The particles with a given energy and a given angular momentum they had in this orbit then fall on the stellar surface and release their energy through nuclear

collisions and plasma effects in a layer with a surface density of less than  $20g/cm^2$ .

Sunyaev and Shakura (1986) calculated the energy release in the disk and in the boundary layer on the stellar surface for a neutron star with negligible rotation. Kluzniak and Wagoner (1985) applied first-order corrections in rotation parameter for particle motion in a gap between the marginally stable orbit and the stellar surface. In this approximation, Hartle and Thorne (1967) found the external gravitational field to be described by the Kerr linearized solution. Miller and Lamb (1996) made an attempt to model the radiation field of a bright thin annulus and estimated the effect of this radiation on particle motion.

The important phenomena, which was n’t taken account in previous works, is the oblateness of the fast rotating self gravitating gaseous masses (like Macloren spheroids).

The gravitational field outside a rapidly rotating flattened neutron star differs markedly from the external field of black holes described by the Schwarzschild and Kerr solutions. For the gravitational field of a real star to be determined, the problem as a whole must be solved for a specified equation of state of the neutron star. It is quite clear that the

complete formulation can be realized only by using powerful computational techniques and sophisticated numerical methods. The fullest known numerical results can be found in the fundamental paper by Cook et al. (1994). The tables in this paper give, in particular, the radii of the marginally stable orbit for corotating and counterrotating disks, equatorial radius, gravitational mass, angular momentum, forward and backward redshifts at the edges of the equator as a function of angular velocity of the neutron star for various equations of state of neutron stars (A, AU, FPS, L, M) which were proposed, in particular, by Pandharipande (1971), Arnett and Bowers (1977), Friedman and Pandharipande (1981), Lorenz et al. (1993), and Wiringa et al. (1988). The stellar *rest* mass was fixed: for normal sequences, it was chosen so that the stellar gravitational mass was equal to  $1.4M_{\odot}$  in the static limit; for maximum mass normal sequences, it was chosen from the condition that stability be lost in the static limit. The results of Cook et al. (1994) were in agreement with the previous numerical results of Friedman et al. (1986).

In contrast to Sunyaev and Shakura (1986), Kluzniak and Wagoner (1985), and Miller and Lamb (1996), we use a global analytical approximation of the metric of the external field of a rapidly rotating neutron star by an exact solution of the Einstein equations in vacuum, which is entirely specified by the stellar mass  $M$ , its angular momentum  $J$ , and the quadrupole moment of the mass distribution  $b$  (the multipole moments are defined in Sect. 3). For  $b = 0$ , this solution transforms to the Kerr solution. We determined the dependence of the quadrupole moment  $b$  on the dimensionless rotation parameter  $j = cJ/Gm^2$  for a given equation of state by comparing the analytically calculated radius of the marginally stable orbit with the numerical data of Cook et al. (1994). It turned out that there were essentially no multipole moments higher than the quadrupole in the external gravitational fields of rotating neutron stars.

The stellar rotation parameter cannot be greater than the critical value  $j_{cr}$  at which the particle velocity on the stellar equator is equal to the Keplerian velocity at the same radius, because, in this case, centrifugal forces begin to strip matter off the star. On the other hand, Keplerian orbits are stable only if their radius is greater than the radius of the marginally stable orbit of corotating particles (this radius is less than or equal to  $3r_g$ ). At critical values of the rotation parameter, the equatorial radius of a compact star is equal to the radius of the marginally stable Keplerian orbit. In this case, the region of free fall of accreted matter disappears. For  $1.4M_{\odot}$  normal sequences, the stellar equatorial radius can be smaller than the radius of the marginally stable orbit only for relatively soft equations of state (EOS A, AU, FPS); the softer is the equation of state, the greater is  $j_{cr}$  ( $j_{cr} = 0.4$  for EOS A,  $j_{cr} = 0.24$  for EOS FPS).

In hundreds of millions (or maybe even billions) of years, accretion onto a neutron star

can increase its mass up to a maximum possible value which becomes unstable in the static limit. For maximum mass normal sequences, the region of free fall of accreted matter exists for all equations of state; the critical rotation parameter is approximately equal to 0.65 for the equations of state we considered (EOS A, AU, FPS, L). For maximum mass normal sequences, the external gravitational field differs only slightly from the Kerr field, while for  $1.4M_{\odot}$  normal sequences, the deviation from the Kerr solution is significant.

The case of a corotating disk in binary systems is natural, because the accreted matter transfers its angular momentum to the star, forcing it to rotate in the same sense. However, the case of a counterrotating disk is also possible: if a binary system in a globular cluster undergoes a strong interaction (a collision) with a third star, it can knock one of the stars out of the binary and form a new pair with the remaining star in which the rotation of the disk is opposite to that of the neutron star.

For particles that rotate in Keplerian orbits in the sense opposite to the stellar rotation (counterrotation), the radius of the marginally stable orbit (greater than  $3r_g$ ) matches the stellar radius at  $j = j_{cr-}$ . We assign the minus sign to  $j$  for a counterrotating disk. For maximum mass normal sequences  $|j_{cr-}| \approx j_{cr}$ .

Thus, we make an attempt to estimate the effect of realistic gravitational fields outside rapidly rotating neutron stars on energy release (we derive explicit formulas for them) when the accreted matter falls on the stellar surface for some equations of state of neutron stars. To this end, we systematically use the exact solution of the Einstein equations which describes the gravitational field of a rapidly rotating object with a quadrupole mass distribution (see Sect. 3 and Appendix 1). Here, we restrict our analysis to  $1.4M_{\odot}$  normal sequences in the static limit and to maximum mass equilibrium sequences. Using the above solution, we study: (i) the luminosities of the accretion boundary layer on the stellar surface and the entire disk; (ii) the dependence of the radial and azimuthal velocity components of the particles at the stellar surface when they fall from the marginally stable Keplerian orbit; and (iii) the dependence of the radius of the marginally stable Keplerian orbit and of the gravitational redshift on dimensionless rotation parameter (see Sect. 1 and 3). For comparison, we give simple relations for the above functions when modeling the stellar external field by the Kerr solution in Sect. 2. Of course, we recognize that radiation begins to affect appreciably the dynamics of accretion at a high luminosity. Below, we provide our model results for luminosities from the accretion boundary layer that are much lower than the Eddington luminosity.

## 1. Formulation of the problem for an arbitrary external axisymmetric field of a rotating neutron star

Space-time is stationary outside a rotating neutron star with axial symmetry, and its metric in the system of coordinates constructed on the orbits of Killing's vectors takes the form (Weil and Papapetru):

$$ds^2 = -f(dt - \omega d\phi)^2 + f^{-1}[\rho^2 d\phi^2 + e^{2\gamma}(d\rho^2 + dz^2)] \quad (1)$$

Here  $\rho, z$  are the Weyl coordinates, for which takes place  $g_{0\phi}^2 - g_{00}g_{\phi\phi} = \rho^2$ . Using the functions  $f, \omega$  we can introduce the single complex valued function-Ernst potential  $\mathbf{E} \equiv f + i\psi$  where the function  $\psi$  is defined by Einstein equation

$$\nabla \cdot \left( \frac{f^2}{\rho^2} \nabla \omega \right) = 0 \quad \Rightarrow \quad \frac{f^2}{\rho} \frac{\partial \omega}{\partial \rho} = \frac{\partial \psi}{\partial z}; \quad \frac{f^2}{\rho} \frac{\partial \omega}{\partial z} = -\frac{\partial \psi}{\partial \rho};$$

Here for convenience the operators of divergence and of gradient  $\nabla \cdot, \nabla$  in the cylindrical coordinates of the 3D euclidean space are defined.

From Einstein's equations in vacuum, Ernst (1967) derived the equation :

$$Re\mathbf{E} \nabla^2 \mathbf{E} - (\nabla \mathbf{E})^2 = 0,$$

for which there is an efficient method of solution using a linear integral singular equation with a Cauchy-type kernel (Sibgatullin 1991).

The free particles move along geodesics, conserving their energy and angular momentum (due to the symmetry properties of the background geometry):

$$\frac{dx^i}{ds} k_i = -E, \quad \frac{dx^i}{ds} m_i = L$$

where the Killings vectors  $k_i, m_i$  have the components  $(-f, f\omega, 0, 0)$  and  $(f\omega, \rho^2/f - f\omega^2, 0, 0)$  respectively;

$$\frac{dt}{ds} = E \left( \frac{1}{f} - \frac{f\omega^2}{\rho^2} \right) + L \frac{f\omega}{\rho^2}, \quad \frac{d\phi}{ds} = -E \frac{f\omega}{\rho^2} + L \frac{f}{\rho^2}. \quad (2)$$

Let us assume that the field is symmetric about the equatorial plane (this hypothesis can be proved in the Newtonian formulation; see Lamb 1947). For the radial component of the 4-velocity vector of a particle moving in the equatorial plane, we then obtain from (1.2)

$$\left( \frac{dr}{ds} \right)^2 \frac{e^{2\gamma}}{f} = \frac{E^2}{f} - \frac{f}{\rho^2} (L - \omega E)^2 - 1 \equiv V(\rho). \quad (3)$$

### 1.1. The equation for the radius of the marginally stable keplerian orbit

The circular trajectories in the equatorial plane can be found with the help of the conditions  $V(\rho) = dV/d\rho = 0$ , from where one can find the energy and the angular momentum of a circularly rotating particle as a function of its radius:

$$E = \frac{\sqrt{f}}{\sqrt{1 - f^2 x^2 / r}}, \quad L = E(p + \omega), \quad (4)$$

$$p \equiv r(-l + \sqrt{l^2 + m - m^2 r})/n, \quad l \equiv f\dot{\omega}, \quad m \equiv \dot{f}/f, \quad n \equiv f - r\dot{f}.$$

Here dote denotes the derivative with respect to  $r \equiv \rho^2$ .

The radius of the marginally stable orbit can be found with the help of the additional condition  $\ddot{V}(r) = 0$ , or equivalently of the condition of a minimum of energy on the circular orbits. In the explicit form it is

$$r(lmn + \dot{l}n - \dot{n}l)\sqrt{l^2 + m - m^2 r} - (l^2 + m - m^2)(n - r\dot{n}) - rn(\dot{l} + 0.5(\dot{m} - m^2) - r\dot{m}) = 0 \quad (5)$$

### 1.2. Energy release in the accretion disc and in the boundary layer

For the determination of the energy, released at the surface of the neutron star due to striking of the particles falling from the accretion disc, let us assume the particles to be at rest with respect to fluid particles in the outer layer of the star after giving back its angular momentum.

4-velocity of the equatorial fluid particle in the coordinate system (1) has the components  $q(1, \Omega, 0, 0)$  with  $q \equiv \sqrt{f}/\sqrt{f^2 - 2f^2\omega\Omega - (r - f^2\omega^2)\Omega^2}$ . The function  $q$  is equal to the component  $u^0$  of 4-velocity. It should be emphasized that angular velocity  $\Omega$  is constant everywhere in the star for the case of its uniform rotation.

The energy per unit mass of such fluid particle is equal

$$E_0 \equiv f(1 - \omega\Omega)\frac{\sqrt{f}}{\sqrt{f^2 - 2f^2\omega\Omega - (r - f^2\omega^2)\Omega^2}}. \quad (6)$$

Let us assume that the kinetic energy of the falling particles relative to the fluid particles on the stellar surface completely transforms into radiation. In the Newtonian approximation, in which particles fall on the stellar surface from the Keplerian orbit, the emitted energy is  $1/2GM(1 - \Omega/\Omega_K)^2/R$ . Indeed, the laws of conservation of energy and angular momentum

for a neutron star when an accreted particle with a small mass  $m$  falls from a circular orbit on the stellar surface are

$$\delta(I\Omega) = mR^2\Omega_K; \quad \delta(I\Omega^2/2) = m\Omega_K^2 R^2/2 - l_s,$$

where  $l_s$  is emitted energie. The change of the moment of inertia  $I$  is equal  $\delta I = kmR^2$ . The coefficient is  $k = 1$ , if the particle remains in the boundary equatorial layer due to centrifugal forces. A more plausible assumption is that the accreted matter spreads over the stellar surface, causing the coefficient  $k$  to decrease. For example,  $k = 2/3$  for the spread over the surface of a sphere and  $k = 2/5$  for a uniform mixing of the accreted matter within a sphere. It thus follows from the law of conservation of energy that  $I\delta\Omega = mR^2(\Omega_K - k\Omega)$ . Therefore, the change in the kinetic energy is equal  $\delta(I\Omega^2/2) = mk\Omega^2 R^2/2 + m\Omega R^2(\Omega_K - k\Omega) = m\Omega_K^2 R^2/2 - l_s$ . Hence, the formula for the emitted energy when a particle falls from a Keplerian orbit to the surface is  $l_s = mR^2(\Omega_K - \Omega)^2/2 - (1 - k)\Omega^2/2$ . In what follow we assume the coefficient  $k$  to be equal to 1.

In general relativity, if the stellar radius is greater than the radius of the marginally stable orbit, the corresponding formulas for the luminosity from the accretion boundary layer on the stellar surface and from the entire disk surface are:

$$L_s = \dot{M}c^2(F - 1)E_0, \quad L_d = \dot{M}c^2(1 - E), \quad (7)$$

where  $mc^2E_0$  is the energy of the particle lying on the star surface, given by formula (4) and  $F \equiv (1 - \Omega(p + \omega))qE$ . Here, we use the fact that the scalar product  $F$  of the 4-velocity of the particle in a Keplerian orbit with the components  $E((1 + f^2\omega p/r)/f, fp/r, 0, 0)$  and the 4-velocity of the particle on the stellar surface has the meaning of energy of a particle in a Keplerian orbit in a tetrad that is fixed relative to the surface of a rotating star.

When the radius of the marginally stable circular orbit is greater than the stellar radius, the energy emitted by the falling particles from the boundary layer per unit time is given by

$$L_s = \dot{M}c^2(F_* - 1)E_0, \quad F_* \equiv (1 - \Omega(p_* + \omega_*))qE_*. \quad (8)$$

Here  $mc^2E_*$  is the energy of the particle on the marginally stable orbit.

The gravitational energy emitted from the entire disk (bounded by the last marginally stable orbit in this case) is

$$L_d = \dot{M}c^2(1 - E_*) \quad (9)$$

In general relativity, the rate of increase of the stellar mass is given by

$$\frac{dM}{dt} = \dot{M}E - L_s/c^2 \quad \text{if } R > R_*$$

$$\frac{dM}{dt} = \dot{M}E_* - L_s/c^2 \quad \text{if } R < R_*$$

Here,  $E$  has the meaning of energy of a particle in a Keplerian orbit on the stellar surface [see formula (4)]; formula (7) must be used for  $L_s$  in the first relation. For  $R < R_*$  (in the second relation),  $E_*$  is the particle energy in the last stable orbit, and formula (8) must be used for  $L_s$ . Thus, when calculating the rate of increase of the mass, we must take into account the losses by radiation, which can reach half the rest energy of the accreted particles (see the end of Sect. 3 for a discussion of this problem).

The rate of increase of the kinetic moment in general relativity is given by

$$\frac{dI\Omega}{dt} = \dot{M}L$$

The length of the stellar equator divided by  $2\pi$  is

$$R = \sqrt{g_{\phi\phi}} = \rho/E_0. \quad (10)$$

For this reason, we use below this circumferential stellar radius. In addition, this quantity, which has an invariant geometrical meaning, is used in theoretical studies of equilibrium of rotating neutron stars.

We emphasize that, in stationary and axisymmetric pseudo-Riemann spaces, the notions of energy and angular momentum have an exact meaning, and that the written expressions for the luminosities are given for the radiative energy that goes to pseudo-Euclidean infinity (if we ignore absorption in the disk).

### 1.3. Physical components of the particle's 4-velocity falling in the gap

If the stellar equatorial radius is smaller than the radius of the marginally stable orbit, then the particles in the gap fall on the stellar surface in helical trajectories, conserving their energy and angular momentum they had in the marginally stable orbit. The physical components of the 4-velocity of the particles in a ZAMO (zero angular momentum observer) tetrad that does not rotate relative to a distant observer are given by

$$V_\phi = \frac{f(p_* + \omega_*)}{\sqrt{r}(1 + f^2\omega(p_* + \omega_* - \omega)/r)}, \quad (11)$$

$$V_r = \sqrt{1 - \omega^2 f^2/r} \frac{\sqrt{1 - f^2(p_* + \omega_* - \omega)^2/r - (1 - f_*^2 p_*^2/r_*)f/f_*}}{1 + f^2\omega(p_* + \omega_* - \omega)/r}, \quad (12)$$



$$\frac{1}{\sqrt{1-V^2}} = \sqrt{f_*/f} \frac{1 + f^2\omega(p_* + \omega_* - \omega)/r}{\sqrt{(1 - \omega^2 f^2/r)(1 - f_*^2 p_*^2/r_*)}} \quad (13)$$

#### 1.4. Gravitational redshift

Let  $Z_b, Z_f$  be the backward-equatorial and the forward-equatorial redshift. The straightforward calculations gives for the magnitude  $Z \equiv (1 + Z_b)(1 + Z_f)$  the expression through the metric coefficient  $f$ :

$$Z = 1/f \quad (14)$$

#### 1.5. Some remarks

Thus, the problem reduces to the choice of an appropriate geometry outside the rotating neutron star. For a global analytical approximation of the results of the numerous numerical calculations in the fundamental paper of Cook et al. (1994), we treat these data as follows (see Fig. 1 and Tables 1-3). The dimensionless rotation parameter  $j \equiv cJ/(GM^2)$  (here,  $c$  is the speed of light;  $G$  is the gravitational constant; and  $J$  and  $M$  are the angular momentum and mass of the neutron star, respectively) is plotted along the horizontal axis. The dimensionless circumferential radius of the marginally stable orbit is plotted along the vertical axis; we assign the minus sign to  $j$  for orbits that rotate in the sense opposite to the disk rotation and the plus sign for orbits that rotate in the same sense.

The treatment of three different theoretical equations of state of neutron stars for normal sequences with a rest mass of  $1.4M_\odot$  (EOS A, EOS AU, and EOS FPS) yields very close curves. The solid line corresponds to the circumferential radii of the marginally stable orbits in the Kerr solution with various rotation parameters. For the points that correspond to the evolutionary sequence of maximum mass normal sequences (MMNS) of the neutron stars (they are marked by filled triangles), we see a marked deviation from the above series of points for the normal sequences. Remarkably, the points essentially lie on the curve of the Kerr solution for  $j$  in the interval  $(-0.15, 0.15)$ ; the agreement with the Kerr curve is better for the points of MMNS. For larger absolute values of  $j$ , the deviation becomes significant. The deviation from the Kerr geometry is attributable to the appearance of a quadrupole component in the rapidly rotating star which is related to its flattening due to rapid rotation.

## 2. The disc accretion in the Kerr field

Here, we use (as the first step and for comparison) the Kerr solution to describe the external geometry. In this case, the above formulas simplify appreciably. In contrast to Kluzniak and Wagoner (1985), Miller and Lamb (1996), Ebisawa et al. (1991), and Biehle and Blandford (1993), we obtain an explicit parametric representation of the quantities in question for an arbitrary rotation parameter.

The formulas for the energy and momentum of particles (divided by their mass) in circular orbits in the Kerr field are well known (Bardeen et al. 1972):

$$E = \frac{1 - 2x + jx\sqrt{x}}{\sqrt{1 - 3x + 2jx\sqrt{x}}}, \quad L = M \frac{-2jx + (1 + j^2x^2)/\sqrt{x}}{\sqrt{1 - 3x + 2jx\sqrt{x}}}, \quad x \equiv M/\tilde{\rho} \quad (15)$$

Thus defined variable  $x$  is used only in this section. Here, we adopt a system of units in which  $G = c = 1$ ,  $\tilde{\rho}$  is the radial Boyer-Lindquist coordinate in the Kerr metric. The radius of the marginally stable orbit can be determined from the condition of minimum of  $E$  as a function of  $x$ . We will not express the radial coordinate  $x$  of the marginally stable orbit as a function of  $j$  (see an explicit formula with cubic radicals in Novikov and Frolov 1986), because this would lead to cumbersome expressions. Instead, we will consider the coordinate  $x$  as a parameter and express all the quantities of interest in terms of this parameter. The expressions for  $j_*$ ,  $E_*$  and  $L_*$  corresponding to the marginally stable orbit are

$$j_* = \frac{4\sqrt{x} - \sqrt{3 - 2x}}{3x}, \quad E_* = \sqrt{1 - \frac{2}{3}x}, \quad L_*/M - jE_* = \frac{1}{x\sqrt{3}}. \quad (16)$$

$x$  changes in the interval  $(1/9, 1/6)$  for the opposite senses of rotation of the disk and the neutron star and in the interval  $(1/6, 1)$  for the same senses of rotation. The corresponding values of  $j$  for the former interval are negative.

Note that, in previous studies of disk accretion, the Schwarzschild metric was used with and without the first term of the expansion in  $j$  (Sunyaev and Shakura 1986; Kluzniak and Wagoner 1985; Ebisawa et al. 1991; and Biehle and Blandford 1993). Our formulas (8) in the Kerr metric hold in any order in  $j$ , because they are exact. As follows from (4), the stellar circumferential radius is given by

$$R/M = x^{-1} \sqrt{1 + j^2x^2(1 + 2x)} \quad (17)$$

The radial coordinate  $r$ , which was introduced in (4), is related to  $x$  in the Kerr solution by

$$r = M^2(1 - 2x + j^2x^2)/x^2$$

In formulas (7)-(9) for the energy release in the entire accretion disk and in the accretion boundary layer, for the metric coefficients in the equatorial plane and the function  $p$ , which is given by (4) and which appears in all formulas for the luminosities, we must substitute their expressions in the Kerr solution:

$$f = 1 - 2x, \quad f\omega = -2Mjx, \quad p = \frac{1 - 2x + j^2x^2}{\sqrt{x}(1 - 2x)(1 - 2x + jx\sqrt{x})}.$$

For the marginally stable orbit, we obtain the following relations for these quantities:

$$f_* = 1 - 2x, \quad f_*\omega_* = 2M(-4\sqrt{x} + \sqrt{3 - 2x})/3, \quad p_* = \frac{4}{3}\left(\frac{1}{\sqrt{x}} - \frac{1}{\sqrt{3 - 2x}}\right).$$

For physical components of velocity in ZAMO tetrad of the particle falling in the gap (preserving energy and momentum corresponding to the circular keplerian motion on the marginally stable orbit) one can obtain the formulas:

$$V_\phi = \frac{2}{\sqrt{27}} \frac{\sqrt{1 + j^2x^2 - 2x}(1 + 2\sqrt{(3 - 2x_*)/x_*})x}{\sqrt{1 - 2x_*/3}(1 + j^2x^2) - 2x^3j/(x_*\sqrt{3})} \quad (18)$$

$$V_r = \frac{\sqrt{1 + j^2x^2(1 + 2x)}\sqrt{2(x - x_*)^3/(3x_*^2)}}{\sqrt{1 - 2x_*/3}(1 + j^2x^2) - 2x^3j/(x_*\sqrt{3})}, \quad (19)$$

$$1/\sqrt{1 - V^2} = \frac{\sqrt{1 - 2x_*/3}(1 + j^2x^2) - 2x^3j/(x_*\sqrt{3})}{\sqrt{1 + j^2x^2 - 2x}\sqrt{1 + j^2x^2(1 + 2x)}}. \quad (20)$$

It should be emphasized that the functions  $V_\phi, V_r, \epsilon$  depending on  $R$  are given parametrically by (9), (11-13).

Finally, let us determine the trajectories of the particles that fall from the marginally stable circular orbit of the accretion disk on the stellar surface. To this end, we use the formulas for the first integrals of motion by dividing the expressions for the  $\phi$  and  $r$  components of the 4-velocity by each other (Bardeen et al. 1972; Novikov and Frolov 1986). We then obtain (by substituting for  $j, E_*$  and  $L_*$  their expressions from (8))

$$\frac{d\phi}{dx} = \frac{2(x - x_*) + \frac{4}{3}(x_* - \sqrt{(3 - 2x_*)x_*})}{\sqrt{2(x - x_*)^3(1 + j^2x^2 - 2x)}}. \quad (21)$$

Substituting  $x = x_* + t^2$ , expanding the right-hand part of (11) in elementary fractions, and performing the integration, we can easily derive a slightly cumbersome expression for  $\phi = \phi(x)$  in explicit form.

Figure 2 shows the trajectories of the falling particles in the coordinates  $X \equiv R(x) \cos(\phi(x))/M$ ,  $Y \equiv R(x) \sin(\phi(x))$  are used, where, instead of  $R(x)$ , the expression ( 9 ) should be substituted. The extreme inner points on these spirals lie on the ergosphere.

### 3. Reconstructing the parameters of a finite-multipole exact solution Einstein equations using numerical results of Cook et al.1994

The external gravitational fields in a stationary axisymmetric case are uniquely specified by Ernst’s potential  $E$  on the symmetry axis (Sibgatullin 1991). Ernst’s potential for the Schwarzschild and Kerr solutions in Weil’s coordinates is

$$\mathbf{E} = \frac{(z - M)}{(z + M)}, \quad \mathbf{E} = \frac{(z + ia - M)}{(z + ia + M)}.$$

It is natural to seek the finite multipole solution at the axes of symmetry in the form

$$\mathbf{E} = \frac{z^n - Mz^{n-1} + \sum_{j=1}^n a_j z^{n-j}}{z^n + Mz^{n-1} + \sum_{j=1}^n a_j z^{n-j}}. \quad (22)$$

The corresponding solution is symmetric about the equatorial plane, if we additionally require that the coefficients with the even subscript  $a_{2k}$  be real (they are determined by the mass distribution and correspond to the Newtonian multipole moments), and that the coefficients with the odd subscript  $a_{2k-1}$  be purely imaginary (they are determined by the distribution of angular momentum in the star and have no analog in the Newtonian theory). For this definition of the multipole moments, the Kerr solution is purely a dipole solution, and its higher multipoles are zero. For other definitions of the multipole moments, the Kerr solution has a fairly complex multipole structure (Hansen 1974; Thorne 1980; Kundu 1981; Simon and Beig 1983). For uniformly rotating stars, the coefficients  $a_{2k-1}$  are most likely equal to zero for  $k > 1$ , with  $a_1 = a \neq 0$ ; this coefficient is equal to the ratio of the star’s angular momentum to its mass. For the fields outside a rotating neutron star, we assume that  $a_{2n} = j^{2n}(\alpha_0^n + \alpha_1^n j^2 + \dots)$ , where  $j = a/M$  is the rotation parameter, i.e., the multipole coefficients are of the order  $O(j^{2n})$ . Therefore, the contribution of the higher multipole moments  $a_{2n}$  at  $n > 2$  is relatively small, because the rotation parameter varies in the range  $|j| < 0.65$  for realistic equations of state of neutron stars.

Using the method of constructing Ernst’s potential in the entire space from its value on the symmetry axis (see Appendix 1), we obtain the solution corresponding to (22)

$$\mathbf{E} = \frac{\Delta_-}{\Delta_+}, \quad \Delta_{\pm} = \det(E_{jk}^{\pm}), \quad (23)$$

Here we introduce the notations

$$E_{jk}^{\pm} = \frac{R_k}{\xi_k - a_j} \pm 1, \quad E_{j+n,k}^{\pm} = \frac{1}{\xi_k - a_j^*}, \quad R_k \equiv \sqrt{r + (z - \xi_k)^2}, \quad j = \overline{1, n}, \quad k = \overline{1, 2n}.$$

The constants  $\xi_k, k = \overline{1, 2n}$  are the roots of the real polynomial of the degree  $2n$ :

$$(z^n + \sum_{j=1}^n a_j z^{n-j})(z^n + \sum_{j=1}^n a_j^* z^{n-j}) - M^2 z^{n-2} = 0,$$

the constants  $a_j, j = \overline{1, n}$  are the roots of the denominator of the  $\mathbf{E}$  on the axes of the symmetry :

$$z^n + Mz^{n-1} + \sum_{k=1}^n a_k z^{n-k} = 0$$

The metric coefficient  $\omega$  is given by formula:

$$f\omega = 2\text{Im} \frac{\Delta_1}{\Delta_+}, \quad \Delta_1 = \det(\Omega_{jk}) \quad (24)$$

Here

$$\Omega_{jk} = \frac{R_k}{\xi_k - a_j} + \frac{1 + R_k + \xi_k - z}{M}, \quad \Omega_{j+n,k} = \frac{1}{\xi_k - a_j^*}, \quad j = \overline{1, n}, \quad k = \overline{1, 2n}$$

It should be remembered that  $\text{Im } A$  denotes the imaginary part of  $A$ ;  $f$  is equal to the real part of  $E$ .

Here, we consider the important case  $n = 2$  [it is the special case of an exact solution to the system of Einstein-Maxwell equations for a rotating charged mass with quadrupole and magnetic moments found by Manko et al. (1994)]. For the quantities on the symmetry axis, we then have

$$\mathbf{E} = \frac{z^2 + (ia - M)z + Mb}{z^2 + (ia + M)z + Mb}, \quad a \equiv Mj. \quad (25)$$

The coefficient  $b$  can be interpreted as a true quadrupole. The metric coefficients  $f, \omega$  in the equatorial plane are given by

$$f = \frac{A - B}{A + B}, \quad \omega/M = -\frac{2jC}{A - B}, \quad A \equiv (r_+ + r_-)^2 r_+ r_- - b, \quad B \equiv (r_+ + r_-)(r_+ r_- - b + r). \quad (26)$$

Here

$$C \equiv (r_+ + r_-)(r_- r_+ + r) + b, \quad 2r_{\pm} \equiv \sqrt{4r + (\sqrt{1 - j^2} \pm \sqrt{1 - j^2 - 4b})^2}, \quad r \equiv \rho^2/M^2$$

Let us now calculate the radius of the marginally stable orbit by using formula (26) for the metric coefficients in the equatorial plane. We assume that the rotationally induced higher multipole moments  $a_{2n}$  are of the order  $O(j^{2n})$ . Therefore, we represent the quadrupole coefficient  $b$  as  $b = j^2 k$ , where  $k = \alpha_0 + \alpha_1 j^2$ . The constants  $\alpha_0, \alpha_1$  are to be determined for each fixed rest mass and naturally depend on the choice of a specific equation of state for neutron stars. In this case, it will suffice to use numerical data for the radii of the marginally stable orbits only at two values of  $j$ .

Remarkably, all the other points from the numerical calculations fall on the derived theoretical relation between the radius of the marginally stable orbit and the rotation parameter constructed by using equation (5).

Thus, substituting (26) into (5) and finding its root  $R = R_*$ , we can determine the constants  $\alpha_0, \alpha_1$  by using the numerical values of  $R_*$  only at two values of  $j$  from Cook et al. (1994). By considering  $1.4 M_\odot$  normal sequences for some equations of state, we can adjust the  $\alpha_0, \alpha_1$  coefficients to fit the realistic numerical data as a whole with 5% accuracy. Note that curve (15) for  $R_*(j)/M$ , which was constructed from the Kerr solution, differs markedly from the realistic curves for  $|j| > 0.15$ . Curiously, the realistic curves for  $R_*(j)/M$  and the Kerr curve (15), nevertheless, have a tangency of the first order at  $j = 0$ . This serves as a good illustration of the remarkable observation of Hartle and Thorne (1967) that the external gravitational field of a slowly rotating star is described by the Kerr metric linearized in rotation parameter. For our purpose, we reduced the data of Cook et al. (1994) for each of the three equations of state (EOS A, EOS AU, EOS FPS) and found that the numerical data of Cook et al. (1994) can be closely fitted by choosing  $b = 2.3j^2 + 1.3j^4$  for EOS A,  $b = 2.9j^2 + 1.1j^4$  for EOS AU, and  $b = 3.2j^2 + 1.6j^4$  for EOS FPS [see Tables 1-3 and Fig. 3 with a theoretical dependence  $R_*(j)/M$  for the quadrupole solution with  $\alpha_0, \alpha_1$  corresponding to EOS AU and to the numerical results of Cook et al. (1994). For comparison, the curve that we constructed from the Kerr solution is also shown in this figure.

A comparison of the theoretical and numerical gravitational redshifts  $Z(j) = 1/f$  (13), where  $f$  is the corresponding metric coefficient on the stellar equator, can serve as another independent test of the validity of describing the external field of a rapidly rotating neutron star by the proposed quadrupole solution. Here, we do not have free parameters at all, because  $\alpha_0, \alpha_1$  were already fixed to reconcile the numerical and theoretical data for the radius of the marginally stable orbit. Substituting the numerical values of the stellar equatorial radius and the corresponding values of  $j$  from Cook et al. (1994) into the function  $f$  (26) for a given equation of state, we can obtain the function  $Z = Z(j)$  for the corresponding normal sequence. It can be verified that the values of  $Z$  for the quadrupole solution with the above dependences of the quadrupole moment  $b(j)$  differ from the numerical values of

$Z(j) = (1 + Z_b)(1 + Z_f)$  from Cook et al. (1994) by 0.001 (see Fig. 4 for EOS AU and Tables 1–3). For comparison, the curve that corresponds to the Kerr solution is also shown here.

Let us now consider the case of MMNS for EOS A, EOS FPS, and EOS L. The maximum possible mass in the static limit is  $1.6541 M_\odot$  (the rest mass is  $1.9182 M_\odot$ ) for EOS A,  $1.7995 M_\odot$  (the rest mass is  $2.1028 M_\odot$ ) for EOS FPS, and  $2.7002 M_\odot$  (the rest mass is  $3.229 M_\odot$ ) for EOS L (Cook et al. 1994). The corresponding neutron stars can "survive" only by rotating: they collapse when losing the angular momentum. Remarkably, these sequences have very similar dependences the quadrupole coefficient on rotation parameter:  $b = 0.53j^2 + 2.45j^4$  (EOS A),  $b = 0.7j^2 + 2.3j^4$  (EOS FPS), and  $b = 0.6j^2 + 2j^4$  (EOS L). At these values of the quadrupole coefficient, the difference between the theoretical and numerical radii of the marginally stable orbit is small for the same rotation parameter (see Fig. 5 for EOS A). Note that the difference between the curves for the quadrupole and Kerr solutions is smaller than that for the normal sequences with  $M = 1.4M_\odot$  mentioned above.

Thus, the dimensionless parameters of MMNS with distinctly different rest masses are, nevertheless, very similar. The usefulness of the dimensional theory can be shown for an almost universal dependence of the dimensionless angular momentum (rotation parameter)  $j = cJ/GM^2$  on dimensionless angular velocity  $W = \Omega GM/c^3$ . For all three equations of state of MMNS the curves  $j = j(W)$  that were constructed by using the numerical data of Cook et al. (1994) are essentially coincident (Fig. 6). Note that the functions  $j = j(W)$  depend appreciably on the choice of an equation of state for  $1.4 M_\odot$  normal sequences (Fig. 7). Below, we show that the dimensionless luminosity from the accretion boundary layer and the physical velocity components of the falling particles on the stellar surface in the ZAMO tetrad as a function of rotation parameter depend only slightly on the choice of an equation of state and are described fairly accurately by the Kerr curves for MMNS.

#### 4. Using the analytical solution for a fast rotating star with the quadrupole mass distribution to describe the disc accretion

We can now use our results for a realistic description of the external gravitational fields of rotating neutron stars to study the accretion characteristics (6) and (8)-(11), which are intimately related to the geometry of space-time near rotating neutron stars. Using the stellar dimensionless equatorial radius from Cook et al. (1994) (see Table 1-3), we can obtain realistic estimates for the rate of energy release and, accordingly, for the luminosity and the physical velocity components of the falling particles in the accretion boundary layer on the stellar surface. Clearly, these parameters depend on the rotation parameter, rest

mass, and selected equation of state of neutron stars, because the equatorial radius itself depends on these parameters.

#### 4.1. The velocities of the falling particles on the star surface

Let us first consider the dependence of the radial and azimuthal physical velocity components in the ZAMO tetrad of the particles that fall freely to the star from the marginally stable orbit for  $1.4M_{\odot}$  normal sequences in the static limit on the neutron-star surface. Here, the difference between the calculations that are based on the realistic quadrupole and Kerr geometries is pronounced (see Fig. 8 for EOS A). The curve  $V_r(j)/c$  which corresponds to the "softer" equation of state differs by a smaller amount from the Kerr curve than do the curves with the "harder" equations of state, for which this difference is significant. Clearly, it is the radial velocity component that is responsible for the particle penetration deep into the neutron-star atmospheres. However, the azimuthal velocity component of the particles relative to the stellar surface mainly contributes to the energy release in the accretion boundary layer for a counterrotating disk as well. Incidentally, the difference between the calculated azimuthal velocity component on the surface in the Kerr geometry and the realistic quadrupole component is less impressive than that for the radial velocity component (see Fig. 9 for EOS A). Below, we give quantitative estimates for the maximum radial velocity on the stellar surface (for a counterrotating disk) for the realistic quadrupole geometry:

$$V_{rmax} = 0.119c \quad \text{at} \quad W = -0.0484 \quad (\Omega = -6.94 \times 10^3 \text{1/sec}) \quad \text{for EOS A}$$

$$V_{rmax} = 0.097c \quad \text{at} \quad W = -0.0475 \quad (\Omega = -6.797 \times 10^3 \text{1/sec}) \quad \text{for EOS AU}$$

$$V_{rmax} = 0.073c \quad \text{at} \quad W = -0.0431 \quad (\Omega = -6.175 \times 10^3 \text{1/sec}) \quad \text{for EOS FPS}$$

In the same time in Kerr geometry the maximum values of the radial component of particles on the star surface are following

$$V_{rmax} = 0.094c \quad \text{at} \quad W = -0.0427 \quad (\Omega = -6.12 \times 10^3 \text{1/sec}) \quad \text{for EOS A}$$

$$V_{rmax} = 0.068c \quad \text{at} \quad W = -0.039 \quad (\Omega = -5.6 \times 10^3 \text{1/sec}) \quad \text{for EOS AU}$$

$$V_{rmax} = 0.047c \quad \text{at} \quad W = -0.035 \quad (\Omega = -5.01 \times 10^3 \text{1/sec}) \quad \text{for EOS FPS}$$

As was already noted above, the calculations for MMNS yield a small difference between the physical parameters in the Kerr geometry and their values in the realistic quadrupole geometry (this can also be seen from Fig. 10 for EOS A):



$$\begin{aligned}
 V_{rmax} &= 0.26c \quad \text{at} \quad W = -0.0573 \quad (\Omega = -6.95 \times 10^3 \text{1/sec}) \quad \text{for EOS A} \\
 V_{rmax} &= 0.277c \quad \text{at} \quad W = -0.0655 \quad (\Omega = -6.22 \times 10^3 \text{1/sec}) \quad \text{for EOS FPS} \\
 V_{rmax} &= 0.284c \quad \text{at} \quad W = -0.0677 \quad (\Omega = -5.2 \times 110^3 \text{1/sec}) \quad \text{for EOSL}
 \end{aligned}$$

Compare these data with data in the Kerr geometry

$$\begin{aligned}
 V_{rmax} &= 0.25c \quad \text{at} \quad W = -0.0446 \quad (\Omega = -5.4 \times 10^3 \text{1/sec}) \quad \text{for EOS A} \\
 V_{rmax} &= 0.255c \quad \text{at} \quad W = -0.052 \quad (\Omega = -4.97 \times 10^3 \text{1/sec}) \quad \text{for EOS FPS} \\
 V_{rmax} &= 0.263c \quad \text{at} \quad W = -0.0604 \quad (\Omega = -4.65 \times 10^3 \text{1/sec}) \quad \text{for EOS L}
 \end{aligned}$$

Figure 11 gives an idea of the dependence of the azimuthal velocity component of the falling particles on the stellar surface for a MMNS with EOS A.

#### 4.2. Energy Release in the Boundary Layer on the Stellar Surface

Such large velocities of the falling particles on the stellar surface entail a substantial energy release in the accretion boundary layer. Figure 12 shows a plot of the dimensionless luminosity of the accretion boundary layer on the stellar surface  $L_s/Mc^2$  against the dimensionless angular velocity for EOS A for a  $1.4 M_\odot$  normal sequence, and Fig. 13 shows the dependence of the dimensionless luminosity for a MMNS EOS A. Here, the difference between the curves that were constructed in the Kerr geometry and in the realistic quadrupole geometry is small. The luminosity is equal to zero for the critical dimensionless angular velocity  $W_{cr}$ , because, in this case, the particle velocity on the stellar surface reaches the velocity in a Keplerian orbit. At the same time, the stellar radius reaches the size of the marginally stable Keplerian orbit. The critical dimensionless angular velocity is given by

$$W_{cr} = \frac{f_*^2 p_* / r_*}{1 + f_* \omega_* / r_*} \quad (27)$$

In the Kerr metric, we can explicitly express the critical stellar angular velocity in terms of  $x_0$  [see formulas (16)]:

$$W_{cr} = \frac{3x\sqrt{x}}{3 + 4x - \sqrt{3x - 2x^2}} \quad (28)$$

This result indicates that, if the radius of a neutron star in the static limit is smaller than the radius of the last stable orbit  $3r_g$ , then its angular velocity cannot exceed its critical

value, which is given by the above formulas. Note that the dimensionless critical velocity is completely determined by the dimensionless critical stellar angular momentum  $j_{cr}$ ; this dependence is universal in the Kerr geometry. In the realistic quadrupole geometry, this dependence depends on the choice of an equation of state. For angular velocities greater than the critical value, centrifugal forces begin to strip the outer layers near the equator off the stellar surface. In the formula for  $W_{cr}$ , the functions (26) at  $r = r_*$  must be substituted for  $f$  and  $g$ . From this formula, we can derive the universal dependence  $W_{cr}(j_{cr})$  for a given dependence of the quadrupole moment on the rotation parameter. Since the radius of the marginally stable orbit is greater than  $3r_g$  for a counterrotating disk, the stellar equatorial radius increases to the size of the marginally stable orbit at negative values of  $j_{cr-}$  that exceed  $j_{cr}$  in absolute value. Thus, if the radius of a neutron star in the static limit is smaller than  $3r_g$ , then its rotation parameter can vary only in the range  $|j| < j_{cr}$ .

It follows from our results that, on the surface of a rotating neutron star, up to 50% of the energy flux from the accreted matter  $\dot{M}c^2$  can be liberated for  $1.4 M_\odot$  normal sequences and up to 80% of the energy flux  $\dot{M}c^2$  can be liberated for MMNS of neutron stars. Here, the nature invented the most perfect mechanism for the conversion of total energy of the falling particles (including their rest energy which is given by the Einstein formula  $E = mc^2$ ) into radiation.

For the critical angular velocities of a counterrotating disk, the luminosity from the accretion boundary layer is a factor of 15 greater than the luminosity of the entire disk for EOS A (see fig.14) and is a factor of 12 greater for the harder EOS FPS in the case of  $1.4 M_\odot$  normal sequences. For MMNS, which becomes unstable in the static limit, the luminosity from the accretion boundary layer can exceed the luminosity of the entire accretion disk by a factor of 20! (see fig.15). Thus, the luminosity from the compact region conspicuously dominates over the luminosity from the extended region. As was already noted above, for all the equations of state we studied, the dependence of the luminosities on the dimensionless angular velocity is the same for MMNS.

## 5. Concluding remarks

Studies of the properties of apparent manifestations of neutron stars in general relativity reveals unexpected properties which are lacking in the Newtonian theory. One of such properties is the existence of a region of free fall of the accreted matter from the marginally stable Keplerian orbit (Sunyaev and Shakura 1986).

Another interesting fact is the relatively simple structure of the gravitational fields

outside rapidly rotating neutron stars with relativistic equations of state. As we showed here, the quadrupole solution (see Sect. 3 and Appendix 1) that describes the external fields of these stars provides an excellent fit to the numerical data for the last stable orbit and for the gravitational redshift in the fundamental paper of Cook et al. (1994), which in turn are in agreement with the numerical studies of other authors.

Our results suggest that the Kerr solution is inapplicable for describing the external gravitational fields of rapidly rotating neutron stars with  $1.4M_{\odot}$  in the static limit. Particularly large differences are obtained for the radial velocity components on the stellar surface that were calculated in the Kerr geometry and in the realistic quadrupole geometry.

We showed that the ratio of the luminosities from the accretion boundary layer and the entire disc in the case of counterrotation can reach 12 for normal sequences and 20 for MMNS. These results can be used in interpreting the strong X-ray emission from very compact regions.

We derived theoretical relations between the critical values of dimensionless angular velocity and dimensionless angular momentum when the neutron star become unstable to centrifugal forces.

From the widths of redshifted lines and from the average redshift, we can infer the angular velocity of the neutron star and the gravitational redshift at the stellar equator, respectively. Therefore, we can judge the stellar equation of state from independent observations of these quantities (as we showed here).

### Acknowledgments

We wish to thank I. Sibgatullin for numerous calculations and Dr. M. Gilfanov for help and support, Dr. V. Astakhov and K. O’Shea for help in the English translation.

### References

- Arnett W.D. and Bowers, R.L. // *Astrophys. J., Suppl. Ser.*, 1977, vol. 33, p. 415.
- Bardeen J.M., Press, W.H., and Teukolsky, S.A. // *Astrophys. J.*, @ 1972, vol. 178, p. 347.
- Biehle G. and Blandford R.D. // *Astrophys. J.*, 1993, vol. 411, p. 302.
- Cook G.B., Shapiro S.L., Teukolsky S.A. // *Astrophys. J.*, 1994, vol. 424, p. 823.

- Ebisawa K., Mitsuda K., and Hanawa T. // *Astrophys. J.*, 1991, vol. 367, p. 213.
- Ernst F. // *Phys. Rev.*, 1968, vol. 167, p. 1175.
- Friedman B. and Pandharipande V.R. // *Nucl. Phys.*, 1981, vol. A361, p. 502.
- Friedman J.F., Ibser J.R., Parker L. // *Astrophys. J.*, 1986, vol. 304, p. 115.
- Hansen R.O. // *J. Math. Phys.*, 1974, vol. 15, p. 46.
- Hartle J.B. and Thorne K. // *Astrophys. J.*, 1967, vol. 153, p. 807.
- Kluzniak W. and Wagoner, R.V. // *Astrophys. J.*, 1985, vol. 297, p. 548.
- Kundu, P. // *J. Math. Phys.*, 1981, vol. 22, p. 1236.
- Lamb G., *Hydrodynamics*, Cambridge: Cambridge Univ. Press 1993, 6 Ed.
- Lorenz C.P., Ravenhall D.G., and Pethick, C.J. // *Phys. Rev. Lett.*, 1993, vol. 70, p. 379.
- Manko, V.S., Martin, J., Ruiz E., Sibgatullin N.R., Zaripov M.N. // *Phys. Rev. D*, 1994, vol. 49, p. 5144.
- Miller M.C. and Lamb F.K. // *Astrophys. J.*, 1996, vol. 470, p. 1033.
- Novikov I.D. and Frolov V.P., *Physics of Black Holes*, Dordrecht: Kluwer 1989.
- Pandharipande V.R. // *Nucl. Phys.*, 1971, vol. A174, p. 641.
- Sibgatullin N.R., *Oscillations and Waves in Strong Gravitational and Electromagnetic Fields*, Berlin: pringer, 1991.
- Simon W. and Beig R. // *J. Math. Phys.*, 1983, vol. 24, p. 1163.
- Sunyaev R.A. and Shakura N.I. // *Pis'ma Astron. Zh.*, 1986, vol. 12, p. 286.
- Thorne K.S. // *Rev. Mod. Phys.*, 1980, vol. 52, no. 2, pt. 1, p. 3.
- Wiringa R.B., Fiks V., and Fabroccini A. // *Phys. Rev.*, 1988, vol. 38, p. 1010.

## **Appendix 1. Construction of the finite multipole solution, possessing the plane of symmetry**

The solution of the Ernst equation with prescribed analytical data on an interval at the axis  $\mathbf{E}(\rho = 0, z) \equiv e(z)$  can be reduced to the linear integral equation with the singular

kernel of Cauchy type (Sibgatullin 1991) :

$$\int_{-1}^1 \frac{\mu(\sigma)(e(\xi) + \tilde{e}(\eta))}{(\sigma - \tau)\sqrt{1 - \sigma^2}} d\sigma = 0; \quad \xi \equiv z + i\sigma\rho, \quad \eta \equiv z + i\tau\rho, \quad \sigma, \tau \in [-1, 1]. \quad (A1)$$

Here the integral should be understood in the sense of principal value;  $e(\xi), \tilde{e}(\eta)$  are the analytical extensions in the complex plane by the Riemann procedure of the functions  $e(z), e^*(z)$  given at the real axes.

For uniformity the solution of (A 1) must fulfill the normalisation condition:

$$\int_{-1}^1 \frac{\mu(\sigma) d\sigma}{\sqrt{1 - \sigma^2}} = \pi \quad (A2)$$

The desired function  $\mathbf{E}(\rho, z)$  then is expressed in the form:

$$\mathbf{E}(\rho, z) = \int_{-1}^1 \frac{\mu(\sigma)e(\xi) d\sigma}{\sqrt{1 - \sigma^2}}. \quad (A3)$$

One can represent the rational function  $e(z)$  (22) of finite multipole solution in the form of the partial fractions:

$$e(z) = 1 + \sum_{j=1}^n \frac{e_j}{z - a_j}.$$

The solution of integral equation (A 1) can be sought in the form:

$$\mu(\sigma) = A_0 + \sum_{k=1}^{2n} \frac{A_k}{\xi - \xi_k}. \quad (A4)$$

Having substituted (A 4) in the integral equation (A 1) and equated to zero the coefficients by independant partial fractions one obtains

$$\sum_{k=1}^{2n} \frac{A_k}{(\xi_k - a_j^*)R_k} = 1, \quad A_0 - \sum_{k=1}^{2n} \frac{A_k}{\xi_k - a_j} = 0, \quad j = \overline{1, n} \quad (A5).$$

From (A 2) one gets:

$$A_0 + \sum_{k=1}^{2n} \frac{A_k}{R_k} = 1, \quad R_k \equiv \sqrt{r + \xi_k^2} \quad (A6)$$

The equations (A 5-6) form a closed system of linear algebraic equations of  $2n + 1$  order with respect to unknown  $A_0, A_1, \dots, A_{2n}$ . According (A 3) the solution  $\mathbf{E}(\rho, z)$  can be represented as follows

$$\mathbf{E}(\rho, z) = 1 + \sum_{k=1}^{2n} \frac{A_k}{R_k} \sum_{j=1}^n \frac{e_j}{\xi_k - a_j} \quad (A7)$$

Having substituted the solution of the system (A 5-6) in the (A 7) one obtains the solution, which can be represented in the form of the ratio of the determinants  $\Delta_{\pm}$  (see formula (23)).

The coefficient  $\omega$  in the metric form (1) can be found as follows:

$$\omega f = \frac{2}{\pi} \text{Im} \int_{-1}^1 \frac{\xi \mu(\sigma) d\sigma}{\sqrt{1 - \sigma^2}} \quad (\text{A8})$$

Having substituted  $\mu(\xi)$  in (A 8) by (A 4) one gets

$$\omega f = -2 \text{Im} \left( \sum_{k=1}^{2n} A_k \left( 1 + \frac{\xi_k - z}{R_k} \right) \right)$$

This expression can be represented in the form (24).

## Appendix 2. Tables

In the tables, the angular velocity is in units of  $10^3 s^{-1}$ , the mass is in solar masses, the circumferential radius is in  $GMc^{-2}$ , the indices  $\pm$  correspond to corotation and counter-rotation, and the subscripts  $k$  and  $q$  characterize the corresponding quantities in the Kerr geometry and in our solution with the quadrupole moment chosen for each equation of state.  $Z = (1 + Z_b)(1 + Z_f)$  (where  $Z_b$  and  $Z_f$  are the backward and forward redshifts, respectively) has the meaning of equatorial redshift. For comparison, columns 4-6 give the circumferential radii of the marginally stable orbit for the numerical solution of Cook et al. (1994), the Kerr solution, and the quadrupole solution, respectively. The circumferential radii in column 7, which were taken from Cook et al. (1994), are required to calculate the luminosity from the accretion boundary layer, the velocity component of the falling particles on the stellar surface, and the gravitational redshift. Column 8 gives theoretical gravitational redshifts.

**Table 1. EOS A**

$\Omega$	$M/M_{\odot}$	$j$	$R_*/M$	$R_*^k$	$R_*^q/M$	$R/M$	$Z^q$
6.94	1.417	0.45488	5.1936	4.48	5.20267	5.16	1.664
6.136	1.412	0.38617	5.198	4.71	5.21374	5.	1.691
5.019	1.408	0.3039	5.27	4.99	5.28351	4.86	1.718
3.244	1.403	0.188978	5.4714	5.39	5.47891	4.73	1.744
0.	1.4	0.	6.	6.	6.	4.66	1.758
-3.244	1.403	-0.1889	6.6966	6.57	6.68539	4.73	1.744
-5.019	1.408	-0.3039	7.173	6.97	7.15572	4.86	1.718
-6.136	1.412	-0.38617	7.5327	7.22	7.50714	5.	1.691
-6.94	1.417	-0.45488	7.8451	7.43	7.833777	5.16	1.664
-7.545	1.421	-0.5151	8.1237	7.62	8.09965	5.33	1.632
-7.954	1.425	-0.56325	8.3567	7.76	8.33841	5.52	1.601
-8.236	1.428	-0.60223	8.5492	7.87	8.52761	5.71	1.570
-8.431	1.431	-0.63346	8.7042	7.97	8.67937	5.94	1.538
-8.591	1.434	-0.66328	8.8592	8.03	8.84255	6.51	1.466

**Table 2. EOS AU**

$\Omega$	$M/M_{\odot}$	$j$	$R_*/M$	$R_*^k$	$R_*^q/M$	$R/M$	$Z^q$
4.457	1.407	0.31113	5.3411	4.96	5.34405	5.24	1.633
3.	1.403	0.20257	5.4807	5.33	5.48028	5.13	1.649
0.	1.4	0.	6	6	6	5.05	1.660
-3	1.403	-0.20257	6.7787	6.65	6.76061	5.13	1.649
-4.457	1.407	-0.31113	7.2535	6.95	7.2307	5.24	1.633
-5.632	1.412	-0.40860	7.7077	7.25	7.6751	5.40	1.609
-6.285	1.416	-0.46983	7.9992	7.44	7.9720	5.54	1.590
-6.797	1.42	-0.52340	8.2569	7.6	8.2397	5.69	1.571
-7.201	1.423	-0.57129	8.4961	7.79	8.4792	5.86	1.546
-7.482	1.426	-0.60883	8.6835	7.84	8.6668	6.04	1.524
-7.713	1.429	-0.64363	8.8572	7.98	8.8594	6.28	1.495
-7.9	1.432	-0.67584	9.0285	8.08	9.0293	6.85	1.432

**Table 3. EOS FPS**

$\Omega$	$M/M_\odot$	$j$	$R_*/M$	$R_*^k$	$R_*^q/M$	$R/M$	$Z^q$
2.284	1.403	0.20337	5.4932	5.33	5.4969	5.37	1.602
0.	1.4	0.	6.	6.	6.	5.27	1.615
-2.284	1.403	-0.2033	6.7927	6.65	6.7753	5.37	1.602
-4.112	1.406	-0.2995	7.2220	6.93	7.203	5.49	1.585
-5.034	1.41	-0.3807	7.6116	7.18	7.5881	5.64	1.566
-5.712	1.414	-0.449	7.9508	7.4	7.9276	5.82	1.544
-6.175	1.417	-0.5022	8.2241	7.57	8.2023	5.99	1.523
-6.544	1.421	-0.5511	8.4795	7.67	8.4615	6.20	1.500
-6.842	1.424	-0.5972	8.73	7.85	8.7131	6.45	1.472
-7.017	1.426	-0.6287	8.8995	7.93	8.8887	6.70	1.445
-7.165	1.429	-0.6593	9.0684	8.02	9.0624	7.36	1.388

**Figure captions**

Fig. 1. The circumferential radius of the marginally stable orbit versus the dimensionless angular momentum. The solid line was constructed for the Kerr solution. The filled circles, open circles, and open triangles correspond to the numerical radii for  $1.4 M_\odot$  normal sequences in the static limit for EOS A, EOS AU, and EOS FPS. The filled triangles represent MMNS with EOS FPS.

Fig. 2. The trajectories of the falling particles in the equatorial plane for a corotating disk for the rotation parameter  $j = 0.22$ . The innermost points correspond to the ergosphere.

Fig. 3. The circumferential radius of the marginally stable orbit versus the rotation parameter for a  $1.4 M_\odot$  normal sequence in the static limit and with EOS AU. Solid and dotted curves correspond to the realistic quadrupole geometry and the Kerr solution, respectively; the dots represent the numerical data of Cook et al. (1994).

Fig. 4. The rotation parameter versus the gravitational redshift  $Z = (1 + Z_b)(1 + Z_f)$  for a  $1.4 M_\odot$  normal sequence in the static limit for EOS AU (solid curve); dotted curve corresponds to the Kerr solution; the dots represent the numerical data of Cook et al. (1994).

Fig. 5. The circumferential radius of the marginally stable orbit versus the rotation



parameter for a MMNS with  $1.6551 M_{\odot}$  in the static limit and with EOS A. Solid and dotted curves correspond to the realistic quadrupole geometry and the Kerr solution, respectively; the dots represent the numerical data of Cook et al. (1994) .

Fig. 6. The function  $j = j(W)$  for MMNS with EOS A, EOS FPS, and EOS L (dashed, solid, dotted curves respectively).

Fig. 7. The function  $j = j(W)$  for  $1.4 M_{\odot}$  normal sequences in the static limit and with EOS A, EOS AU and EOS FPS (dashed, dotted, solid curves respectively).

Fig. 8. The radial physical velocity component of the particles (in the ZAMO tetrad) that fall from the marginally stable orbit on the stellar surface versus the dimensionless angular velocity  $W$  for a  $1.4 M_{\odot}$  normal sequence with EOS A in a realistic gravitational field (solid curve ). Dotted curve corresponds to the Kerr solution.

Fig. 9. The same as Fig. 8 for the azimuthal physical velocity component.

Fig. 10. The radial physical velocity component of the particles (in the ZAMO tetrad) that fall from the marginally stable orbit on the stellar surface versus the dimensionless angular velocity  $W$  for a MMNS with EOS A in a realistic gravitational field (solid curve ). Dotted curve corresponds to the Kerr solution.

Fig. 11. The same as Fig. 10 for the azimuthal physical velocity component.

Fig. 12. The luminosity  $L_s$  from the accretion boundary layer versus the dimensionless angular velocity  $W$  for a  $1.4 M_{\odot}$  normal sequence with EOS A against the background of a realistic gravitational field for  $R < R_*$  (solid curve ). Dotted curve corresponds to the Kerr solution.

Fig. 13. The luminosity  $L_s$  from the accretion boundary layer versus the dimensionless angular velocity  $W$  for a MMNS with EOS A against the background of a realistic gravitational field for  $R < R_*$  (solid curve ). Dotted curve corresponds to the Kerr solution

Fig. 14 The ratio of the luminosities from the accretion boundary layer and the entire disc versus the dimensionless angular velocity  $W$  for a  $1.4 M_{\odot}$  normal sequence with EOS A against the background of a realistic gravitational field for  $R < R_*$  (solid curve ). Dotted curve corresponds to the Kerr solution.

Fig. 15 The ratio of the luminosities from the accretion boundary layer and the entire disc versus the dimensionless angular velocity  $W$  for a MMNS with EOS A against the background of a realistic gravitational field for  $R < R_*$  (solid curve ). Dotted curve corresponds to the Kerr solution.

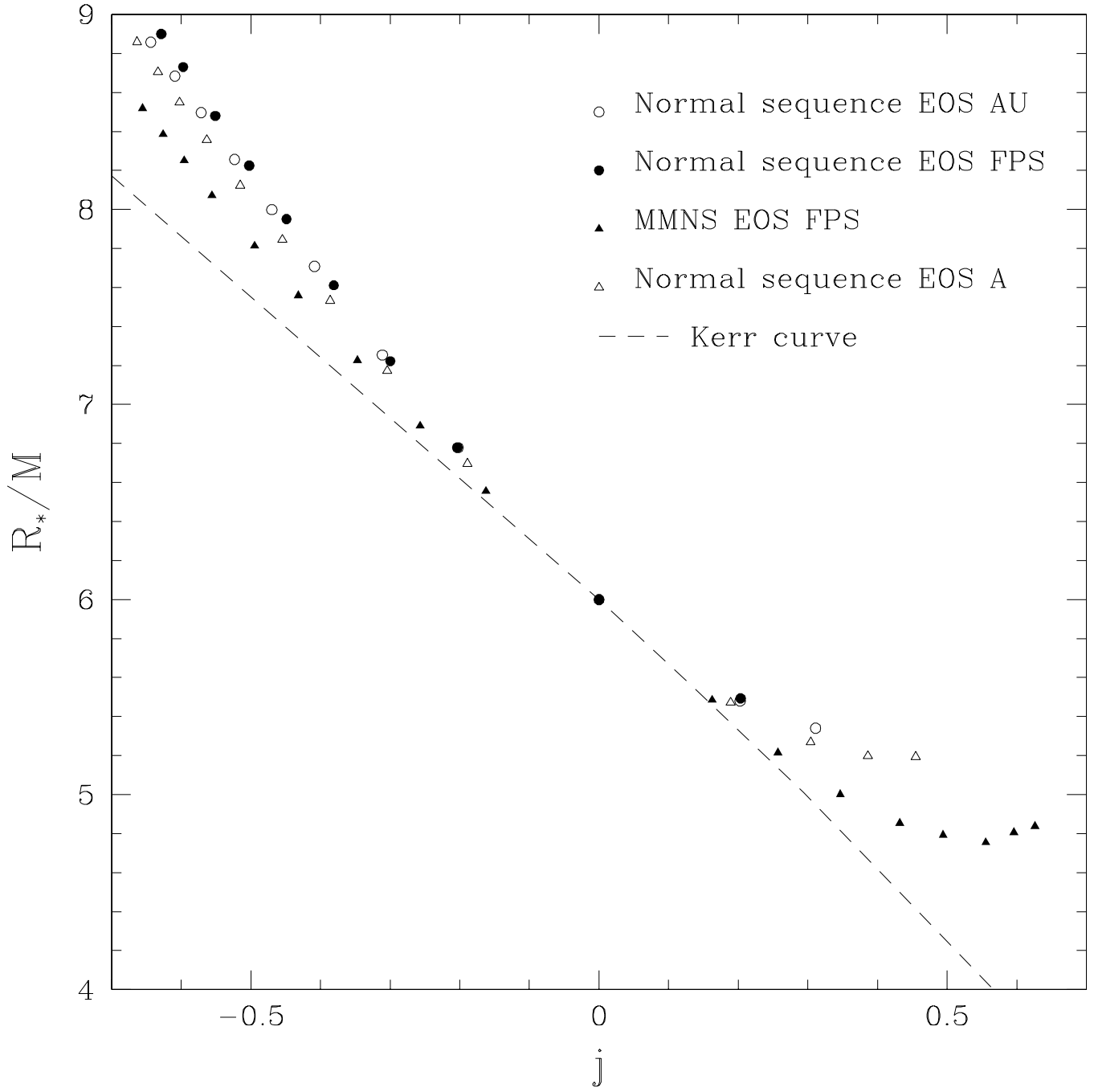


Fig.1

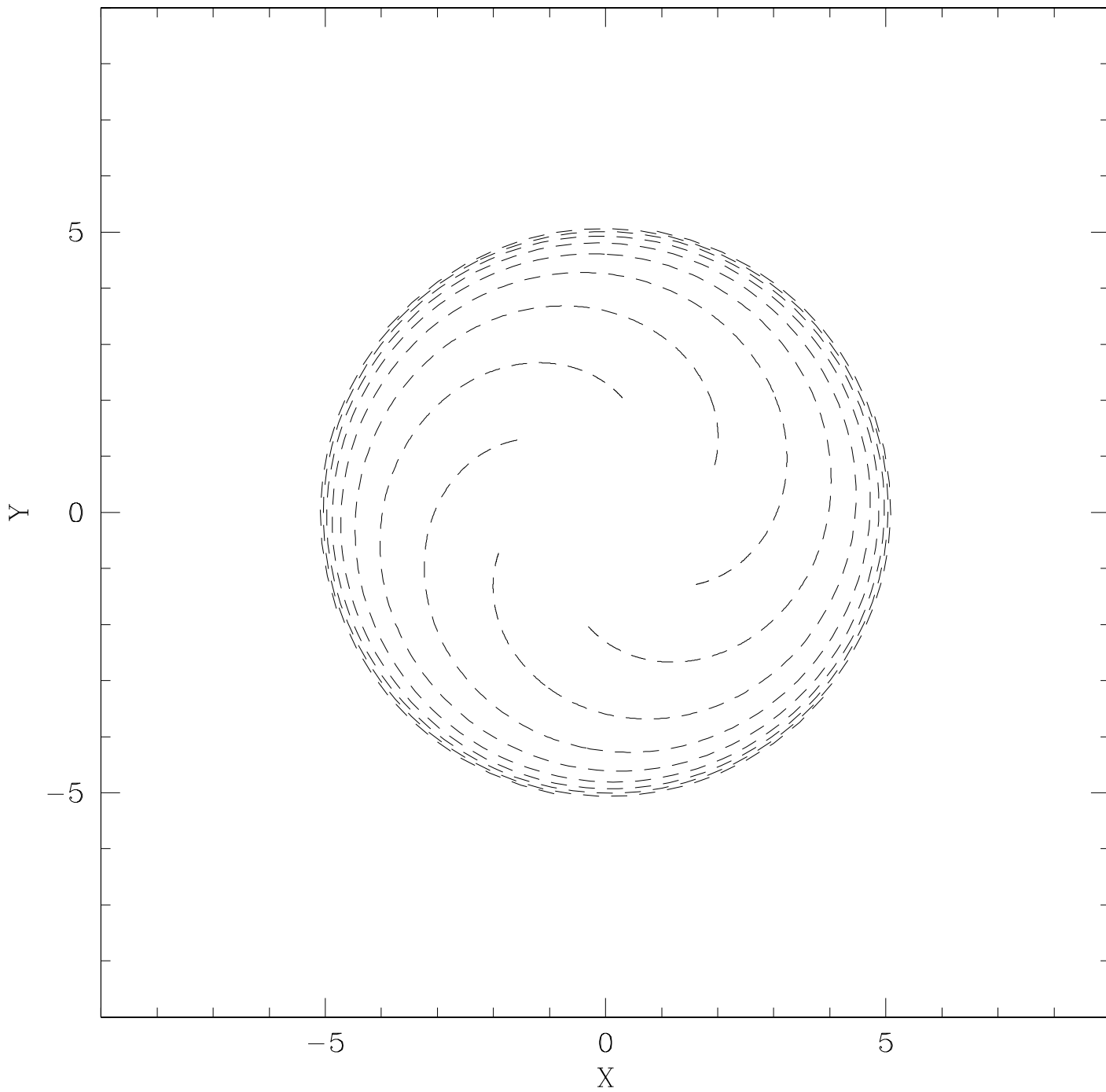


Fig.2

Normal sequence EOS A

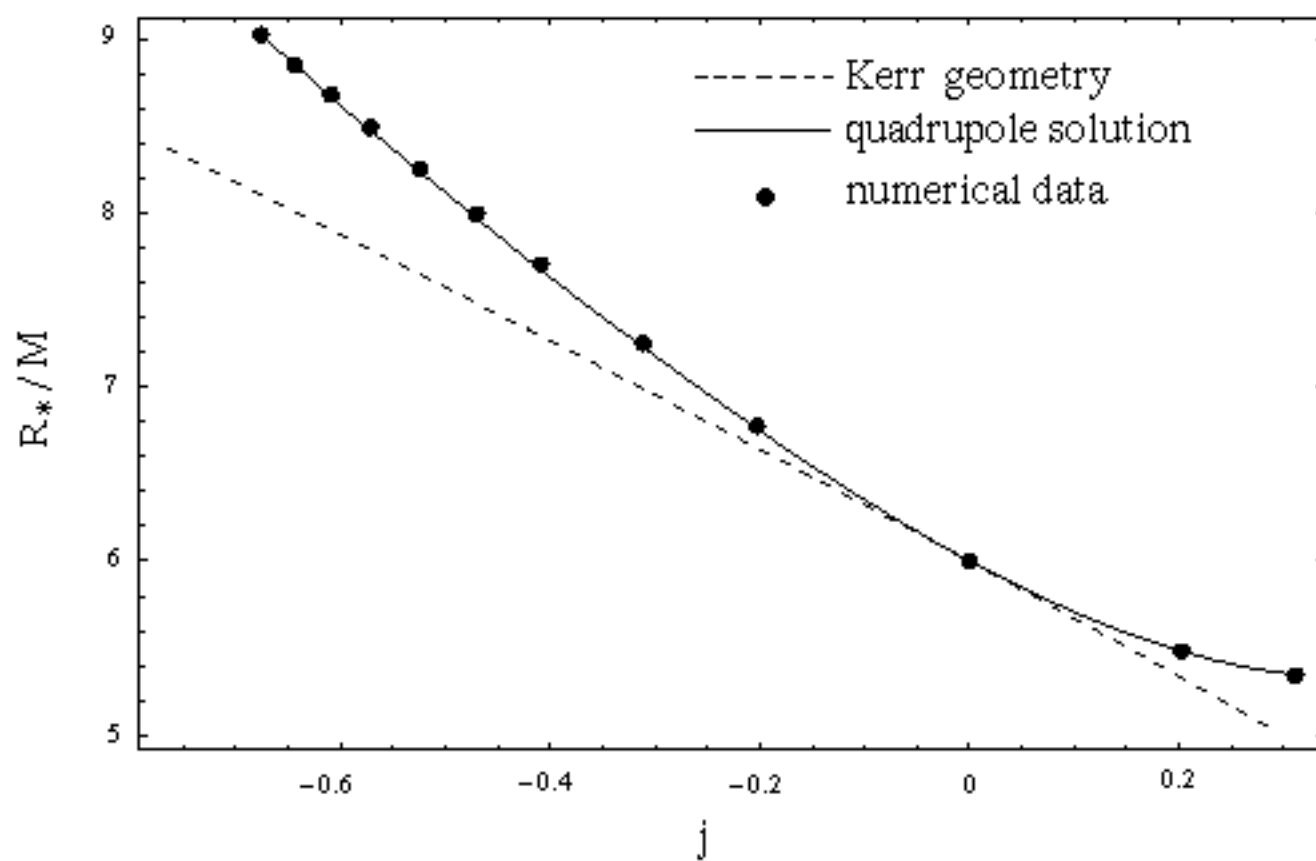


Fig.3

Normal sequence EOS A

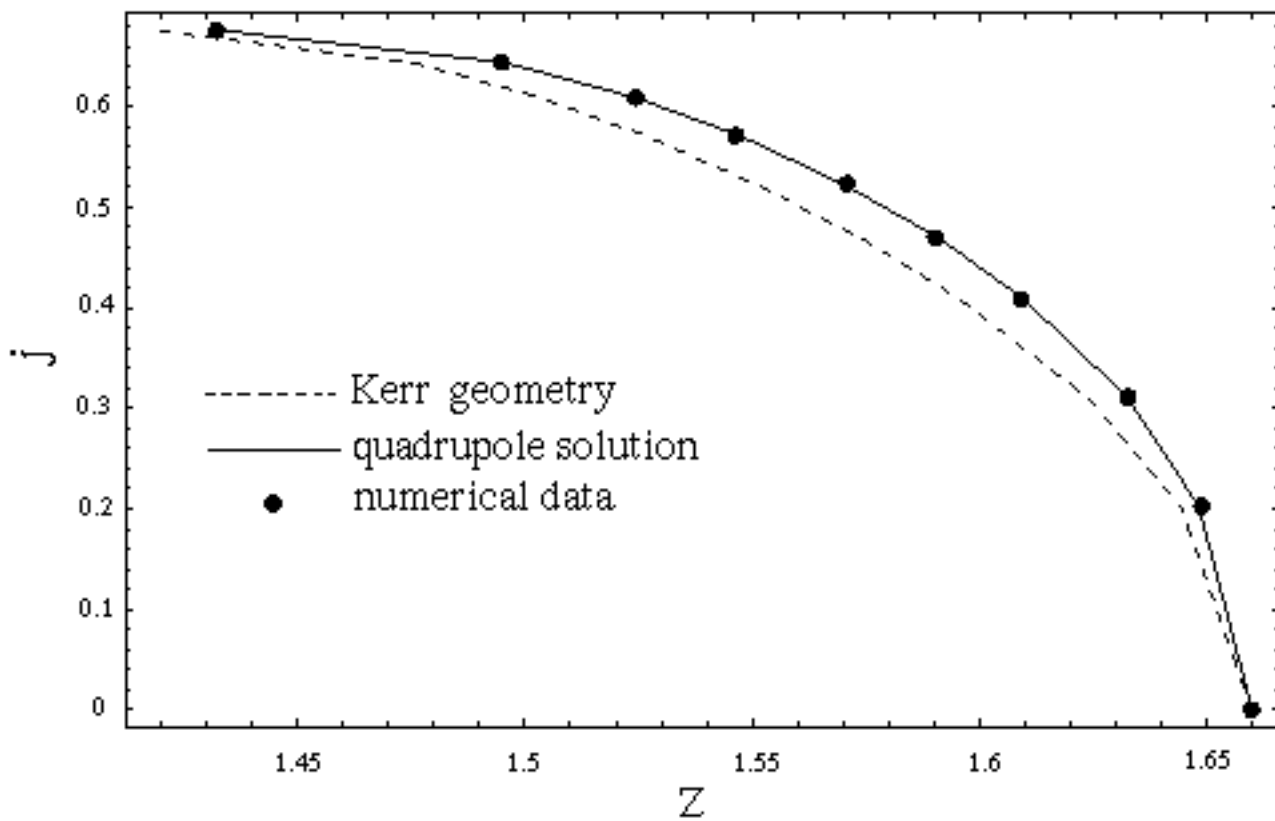


Fig.4

Maximum mass normal sequence EOS A

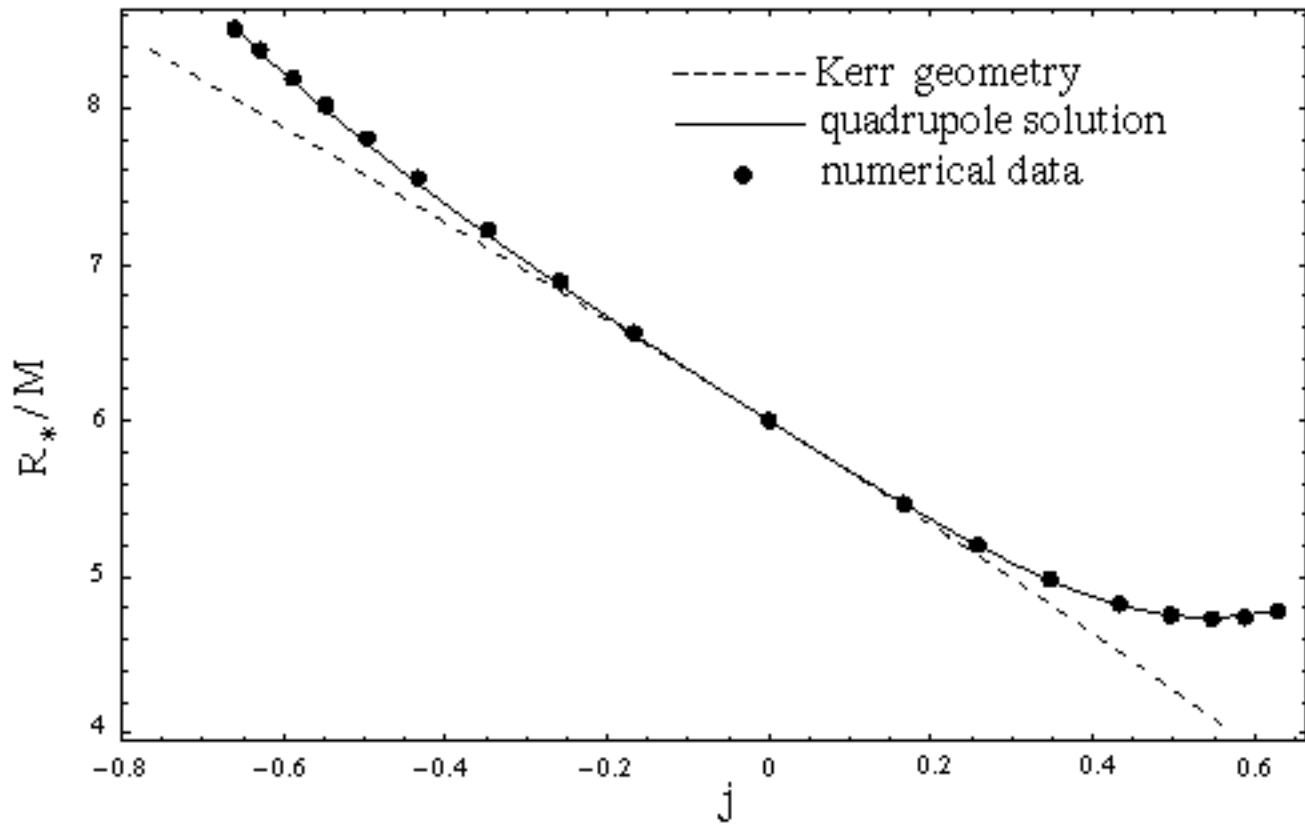


Fig.5

Maximum mass normal sequence EOS A, FPS, L

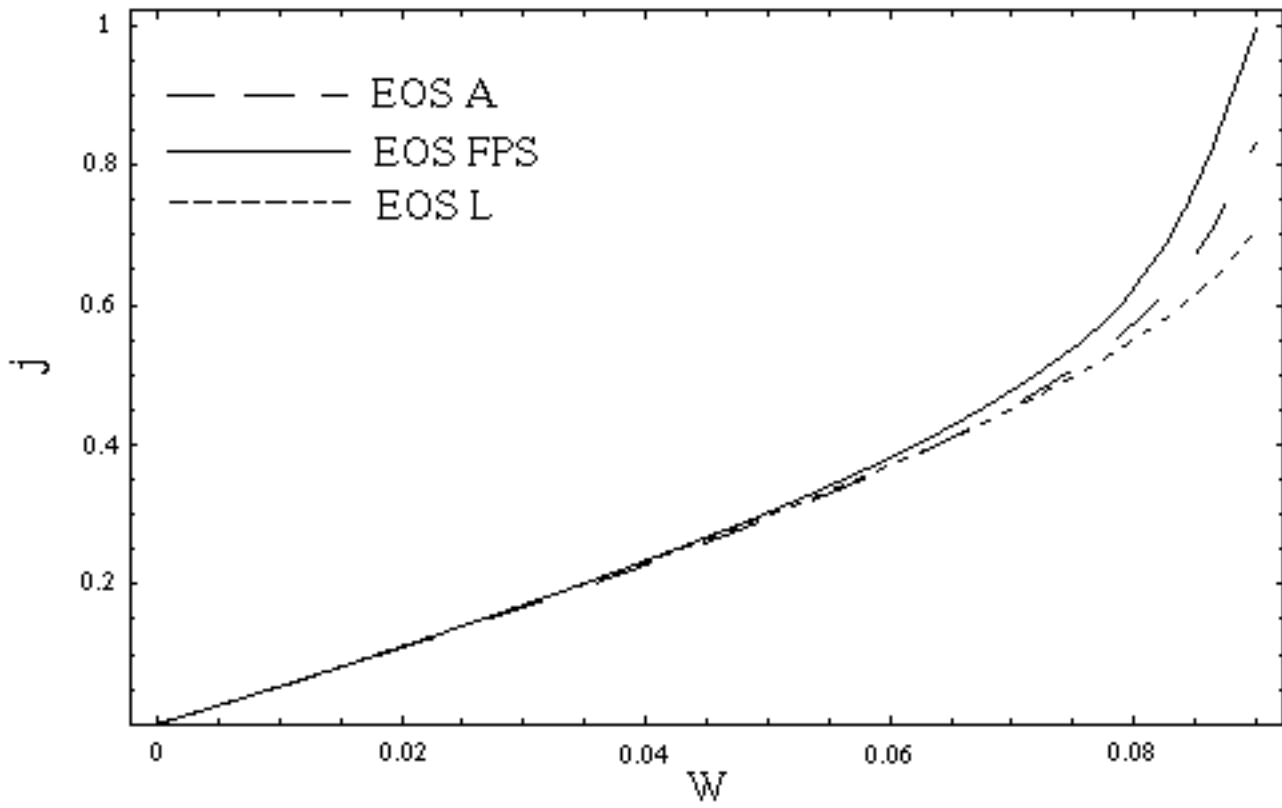


Fig.6

Normal sequences EOS A, AU, FPS

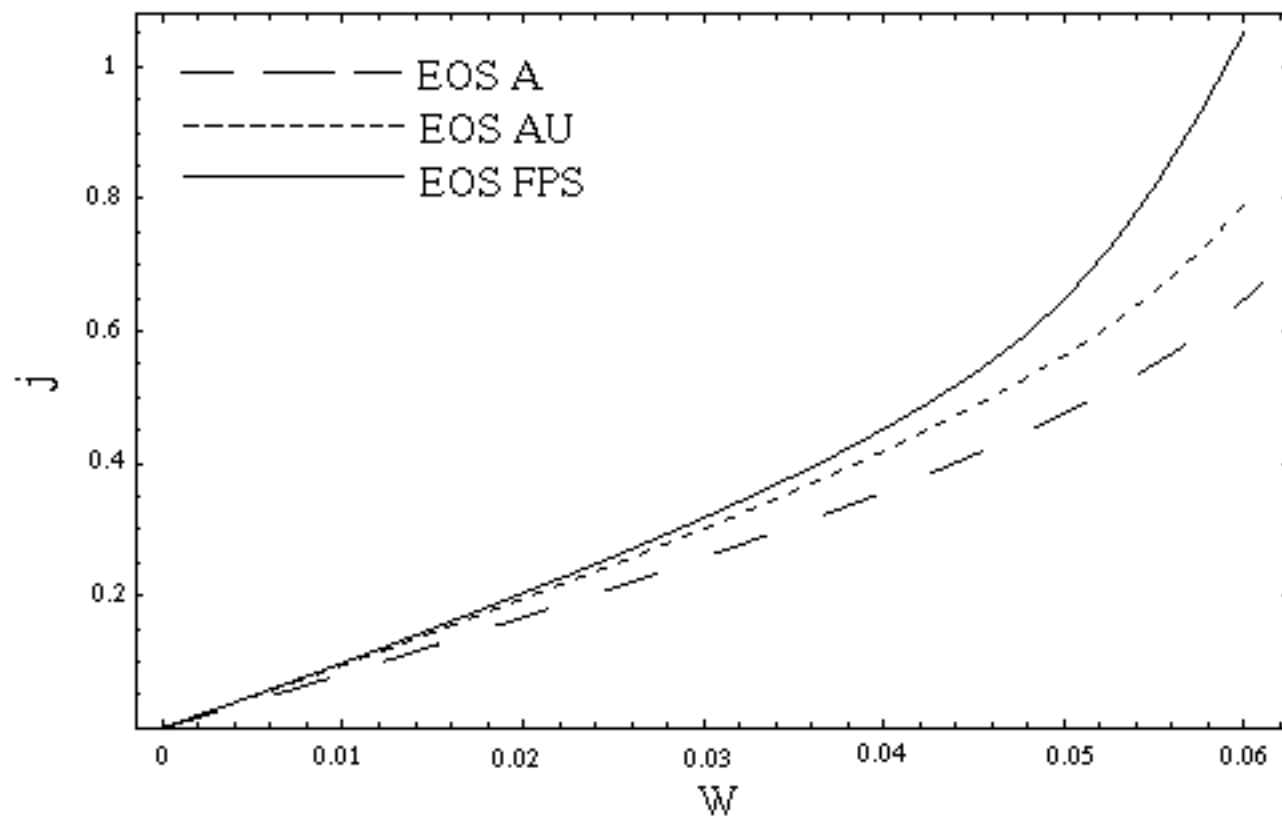


Fig.7



Normal sequence EOS A

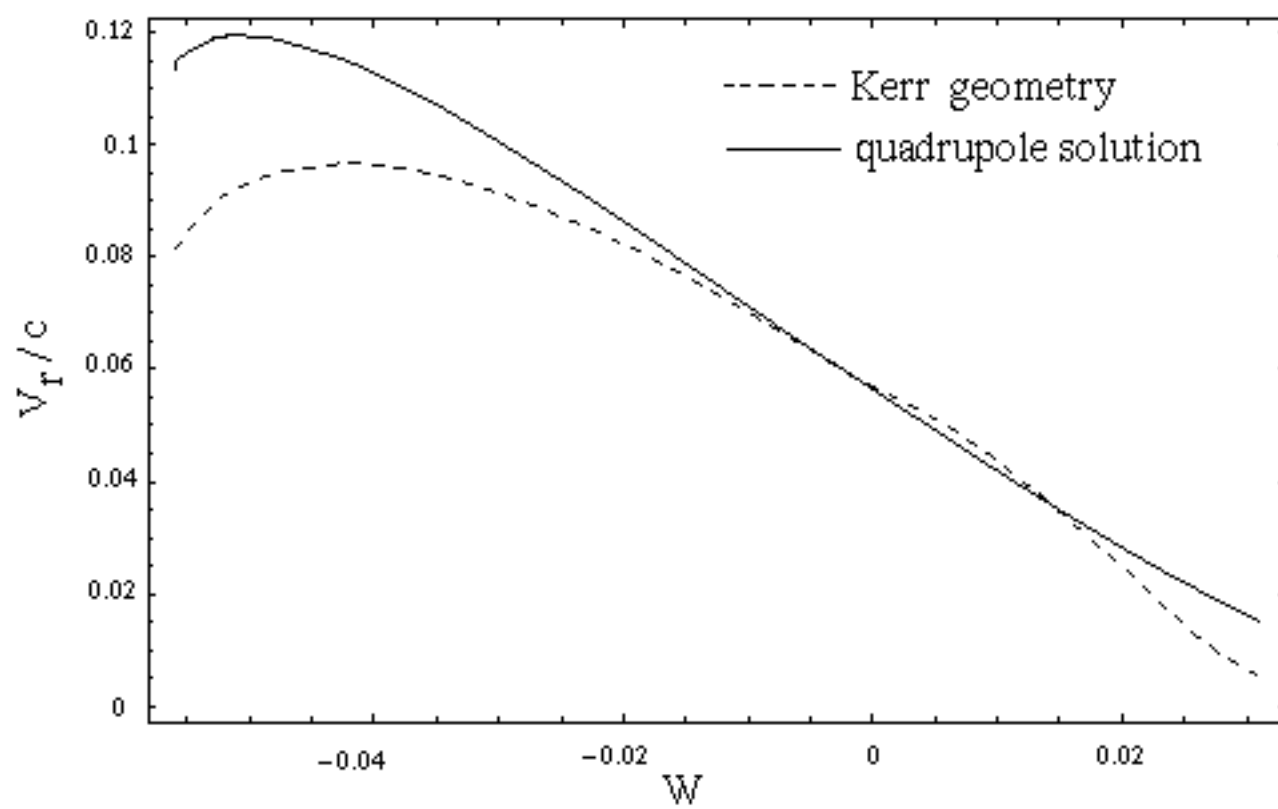


Fig.8

Normal sequence EOS A

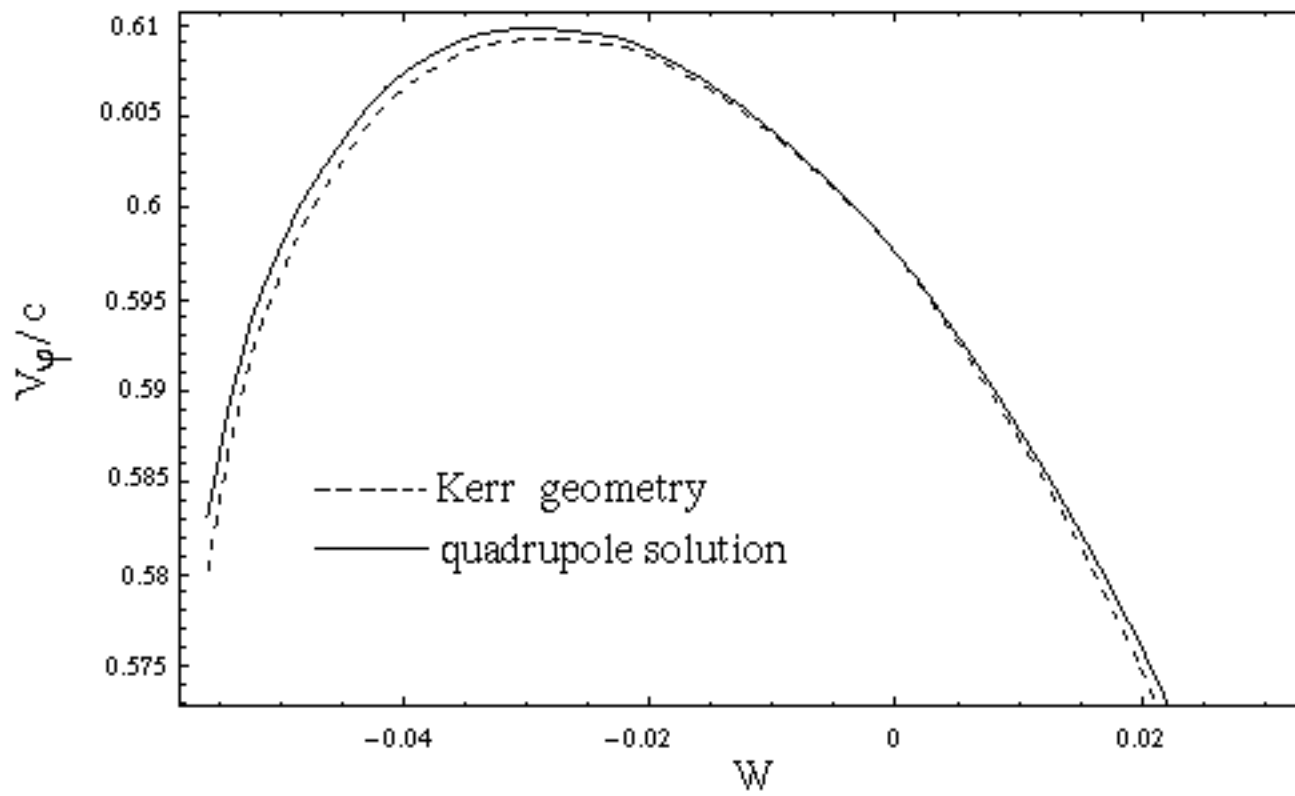


Fig.9

Maximum mass normal sequence EOS A

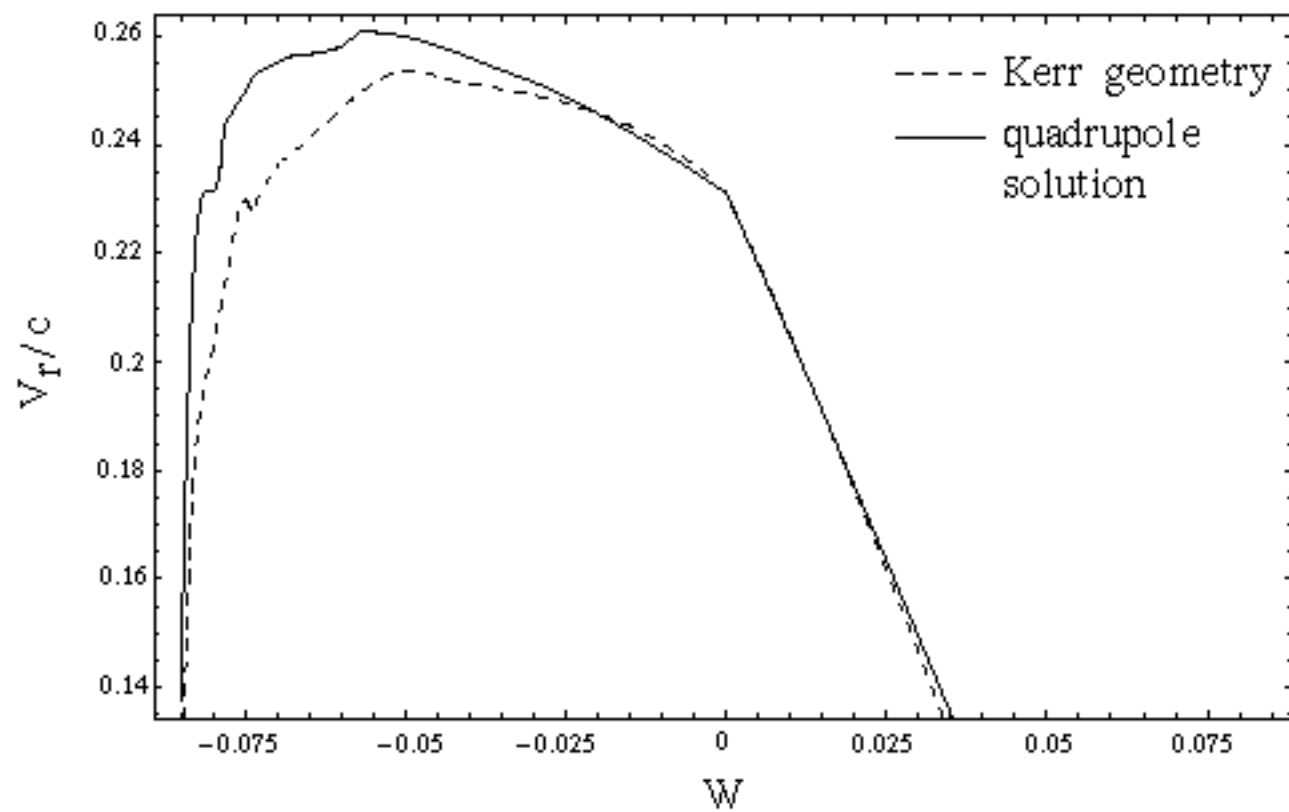


Fig.10

Maximum mass normal sequence EOS A

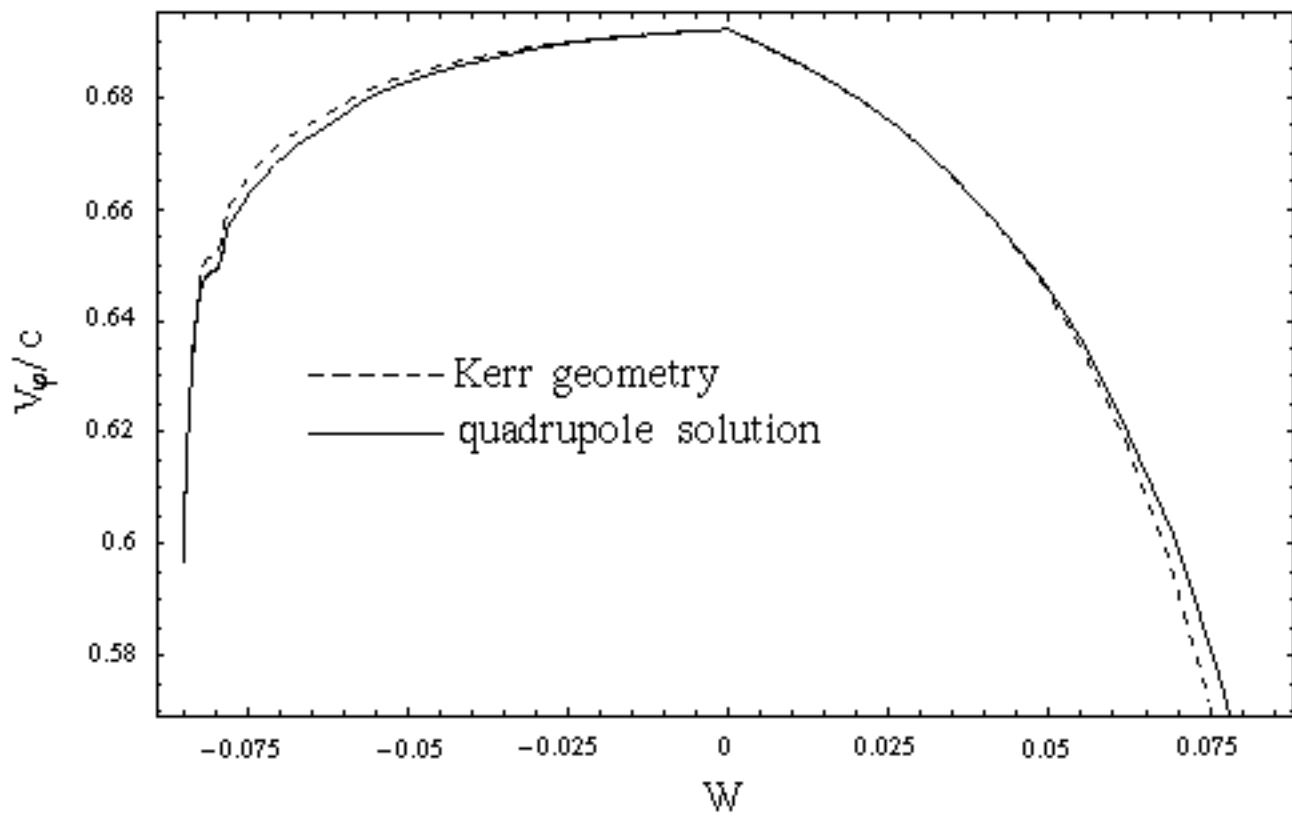


Fig.11

Normal sequence EOS A

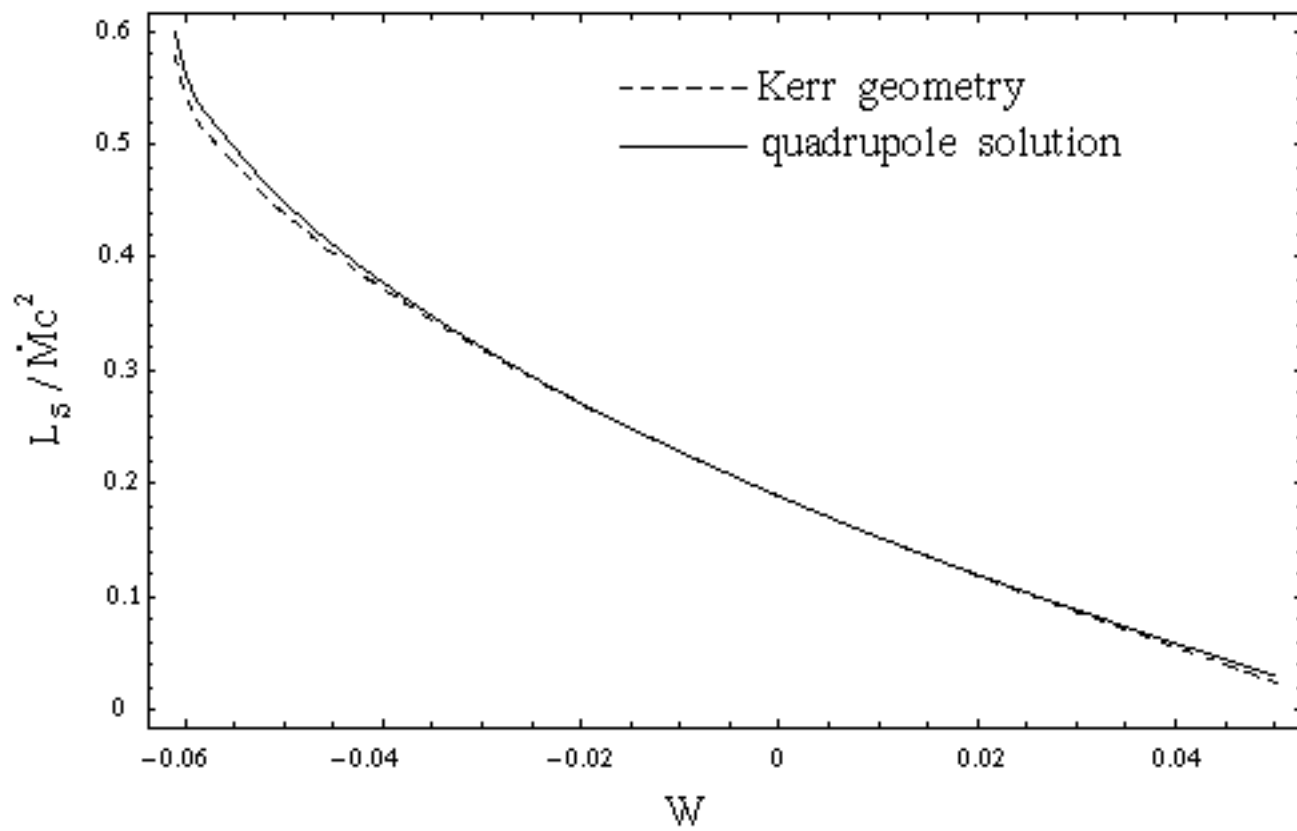


Fig.12

Maximum mass normal sequence EOS A

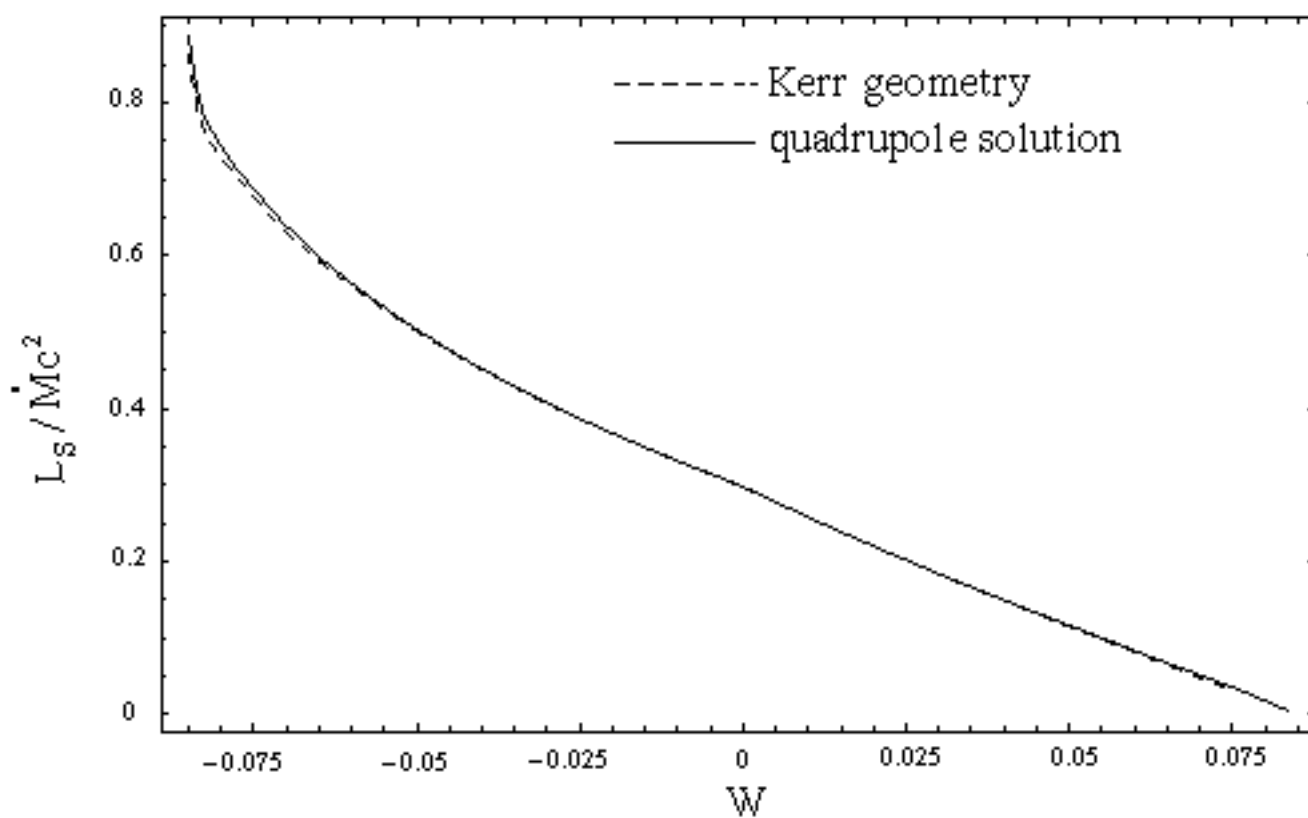


Fig.13

Normal sequence EOS A

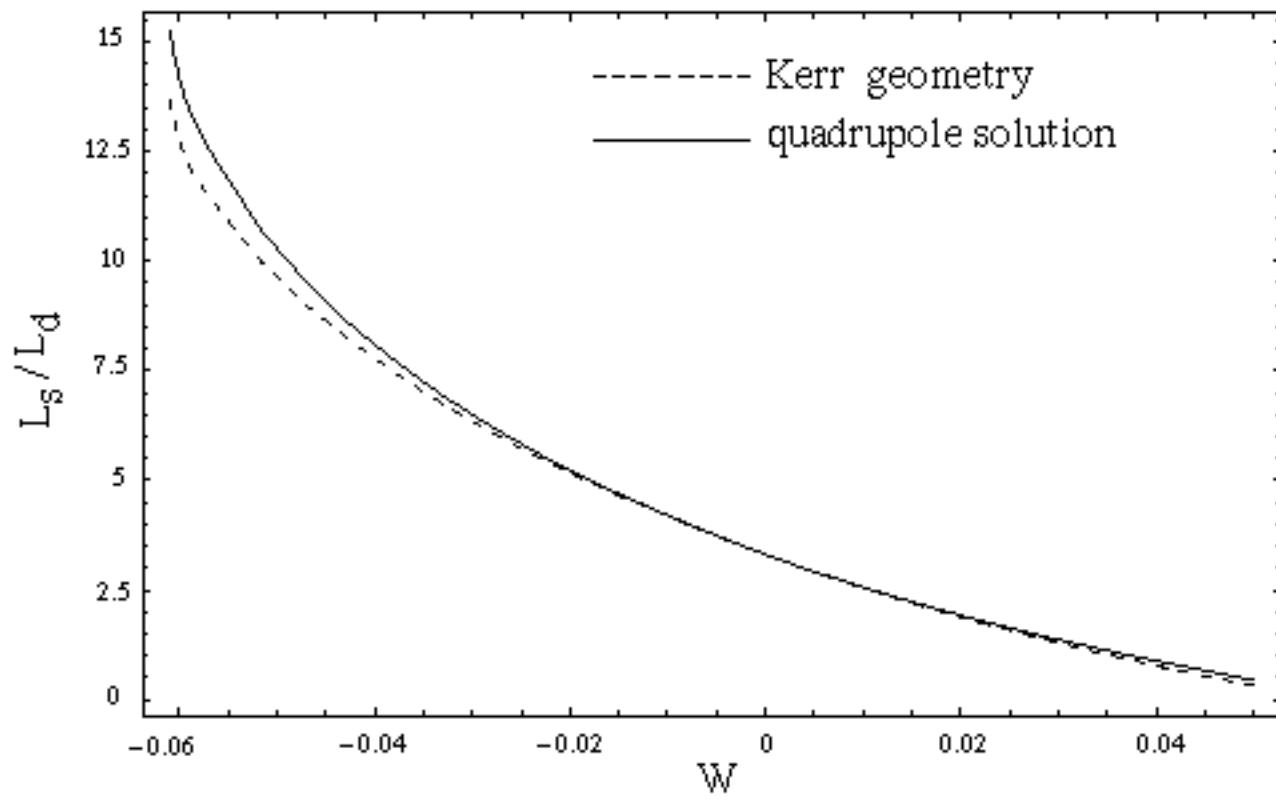


Fig.14

Maximum mass normal sequence EOS A

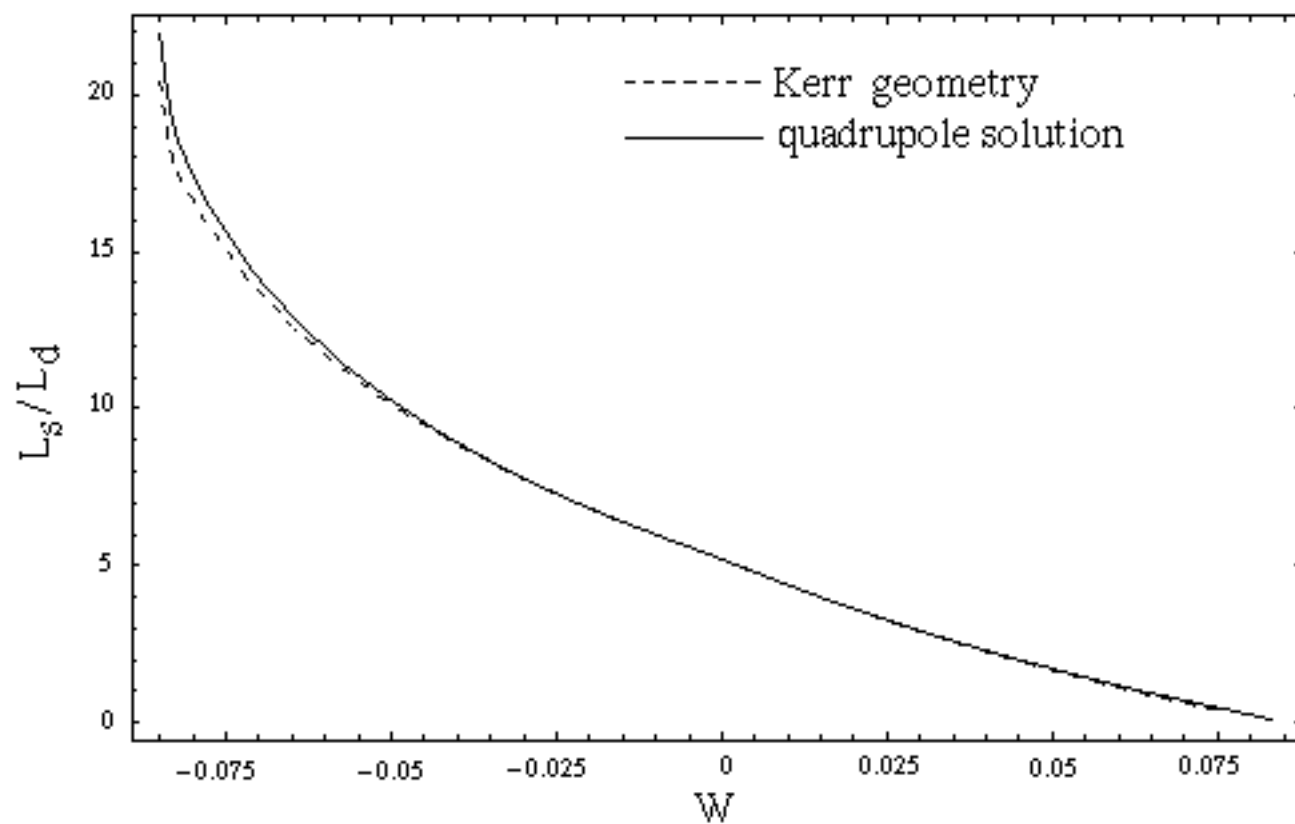


Fig.15